Biological Effects of Antiprotons
Are Antiprotons a Candidate for Cancer Therapy?

Status Report for Experiment AD-4/ACE

Michael Holzscheiter[1,2], Jan Alsner[3], Angelo Angelopoulos[4], Niels Bassler[3,5], Gerd Beyer[6], Rebecca Boll[2], Fred Currell[7], John DeMarco[8], Michael Doser[9], Dragan Hajdukovic[10], Oliver Hartley[6], Kei Iwamoto[8], Oliver Jäkel[5], Ioannis Kantemiris[4], Franz Joachim Kaiser[5], Joy Kavanagh[7], Helge Knudsen[11], Roy Keyes[1], Sandra Kovacevic[10], Søren Pape Møller[11], Jens Overgaard[3], Jørgen Petersen[3], Osman Ratib[6], Hermann Rochus[4], Giuseppe Schettino[7], Stefan Sellner[2], Sara Tegami[2], David Timson[7], Heikki Tölli[12], Brita Singers-Sørensen[3], Timothy Solberg[13], Sanja Vranjes[14], Carsten Welsch[2], Patrick Weber[9], and Brad Wouters[15]

[1] University of New Mexico, [2]Max Planck Institute for Nuclear Physics, Heidelberg
[3]Aarhus University Hospital, [4] University of Athens,[5]Deutsches Krebsforschungszentrum
[6]Geneva University Hospital, [7]Queens University of Belfast , [8]University of California at Los Angeles [9]CERN, [10]University of Montenegro, [11]Aarhus University, [12]University of Umeå, [13]University of Texas, [14]Vinca Institute of Nuclear Sciences, [15]University of Maastricht.

CERN-SPSC-2010-001 / SPSC-SR-054
07/01/2010

Summary

The ultimate goal of radiotherapy for cancer is to eradicate the tumor growth while minimizing the impact on normal tissue. Compared to x-ray therapy, particle beam therapy offers distinct advantages due to the inverse dose profile. The energy deposited along the incoming beam is much reduced compared to x-rays, and virtually no dose is deposited by particle beams beyond the Bragg peak. From the very beginning in 1946 heavy ions were studied in parallel to protons because of the enhanced biological effectiveness, and currently one can observe a strong increase of interest in heavy charged particle therapy, especially in Europe. For similar reasons other, more exotic, particles have been considered for therapy. Pions were studied extensively in the 60's and 70's but eventually abandoned due to the poor dose conformity and the contamination of the beam by decay products. Antiprotons have been proposed on theoretical grounds by Kalogeropoulos and Gray [1] in 1984. Shortly afterwards it has been shown by Sullivan [2] that the physical dose deposition at the end of range is twice that obtained for protons.

Clearly, for all particles considered the simple picture of dose deposition due to the primary beam needs to be augmented by inclusion of secondary particles due to nuclear interactions between beam and target atoms. These not only can cause a modification of the dose profile in the target but also will deposit dose outside the targeted volume. Spectral and geometrical distributions of secondary particles will vary with type of primary particle and complex dose planning tools are being developed to take these effects into account. Due to longer survival times achievable today late effects and secondary cancers caused by the initial therapy are becoming more and more a concern in clinical practice and several large reviews in this field have been published in the last year [3].

In 2003 the AD-4 experiment was initiated to study the biological effectiveness of antiprotons with a focus on potential use in cancer therapy. In addition to the increased physical dose available when using antiprotons it has been postulated that the biological effectiveness in the Bragg peak should be enhanced, as a significant part of the additional energy is deposited by heavy ion

recoils and nuclear fragments. An additional advantage already mentioned by Kalogeropoulos et al. consists in the possibility of real-time monitoring of the actual dose deposition.

A significant concern in antiproton therapy could be the secondary dose due to medium and long-range products of the annihilation events, high-energy pions and gammas, as well as neutrons with a broad energy spectrum. To perform a balanced assessment of the potential of antiprotons for cancer therapy detailed knowledge of physical energy deposition, biological efficiency in the primary beam path, and a full understanding of the mixed radiation field produced by the annihilation events is necessary.

The AD-4/ACE collaboration has been studying the biological effects of antiproton beams on living cells for an integrated beam time of 6 weeks since 2003. Initial experiments using a beam at 46.7 MeV kinetic energy readily available at CERN did show a significant enhancement of the biological effective dose ratio (BEDR) for antiprotons compared to protons. The experimental methods and analysis as well as the definition of terms used here are described by Holzscheiter et al. [4]. Based on this initial success the collaboration requested delivery of a higher energy beam (502 MeV/c), providing deeper penetration into the target and allowing the use of a clinically relevant spread-out Bragg peak (SOBP). We have used this beam setting for four run periods and have collected data on dosimetry of the mixed radiation field produced by the annihilation of antiprotons as well as on cell survival of V79 Chinese Hamster cells and Human FaDu cells (a human epithelial cell line derived from a squamous cell carcinoma of the hypopharynx).

Using dosimetric measurements with ionization chambers and alanine pellets we have successfully benchmarked the FLUKA Monte Carlo code [5], which now allows precise dose planning of the irradiation experiments. Using the calculated dose values along the beam path together with reference measurements using the same materials and methods and a standard ^{60}Co radiation source we can now extract the Relative Biological Efficiency (RBE) instead of using the Biological Effective Dose Ratio (BEDR) utilized in the initial experiments. RBE, while still a complex quantity and dependent on a variety of physical and biological parameters, can be compared more easily across different radiation modalities and can be used to analyze the differences in therapeutic potentials for different radiation qualities.

Early 2007 we also performed a set of irradiations using the same methods and materials at GSI with carbon ions giving the same calculated penetration depth and the same calculated width of the Spread Out Bragg Peak (SOBP) as the antiprotons at CERN.

We have published a number of papers describing the results of the cell survival measurements and the progress on dosimetry and Monte Carlo (see Appendix I). While a continuation of cell survival measurements is necessary to base any assessment of the therapeutic potential of antiprotons and any comparison to other particle beam modalities on a well-founded scientific basis, the collaboration has initiated in parallel work on studying potential detrimental effects on cells placed outside the primary beam area (peripheral effects). Measurements of cell survival beyond the Bragg peak can be used for an initial assessment of the relevance or severity of these effects, but as the relevant biological endpoint in this context is not tumour control but normal tissue complication, other methods that are sensitive to DNA damage on the cellular

level seem more appropriate. Original experiments using a combination of clonogenic survival and the COMET assay to study the incidence of DNA double strand breaks hinted that the out-of-field effects are small [6]. In 2008 we performed a pilot study on the development of foci using the γ-H2AX assay, and based on preliminary results we designed an improved experiment concentrating on a systematic study of cell damage outside the direct beam due to medium and long-range secondary products from the annihilation events. In parallel, these studies were also designed to obtain information on the chemically mediated bystander effect where cells not subject to irradiation show effects due to the irradiation of cells with which they share medium; they are bystanders to the irradiation.

In addition to biological studies we have dedicated a moderate percentage of the available beam time to the development of beam monitor systems and novel dosimetric methods that promise direct measurements of linear energy transfer (LET) in the beam. These methods are not restricted in use to antiprotons but would represent important tools for heavy ion therapy, where RBE variations along the primary beam and within the spread-out Bragg peak (SOBP) are present as well.

Parallel, and completely symbiotic, we have increased our efforts towards real time imaging of the stopping distribution. We have performed a Monte Carlo study [7] showing that the very initial fraction of a typical treatment delivered with antiprotons would be sufficient to obtain a high-resolution image of the actual dose deposition. This would be an invaluable tool to any clinician who faces the uncertainties in depth dose profiles due to inhomogeneities in the target and uncertainties in ionization potential for the complex target materials encountered. Using a silicon pixel detector provided to us by the ALICE collaboration we have obtained first promising experimental results on a simple detector arrangement.

Initial Monte Carlo calculations for realistic treatment situations have been performed, based on physical dose alone [8]. Based on these results and a simplified model on RBE variation vs. depth for antiprotons and carbon ions we have generated generic comparisons between protons, antiprotons, and carbon ions. Using independent optimization of the dose plan for each particle type we have shown that antiprotons not only show a clear improvement compared to protons in terms of secondary dose outside the target volume but also may be superior to carbon ions in terms of medium dose deposition outside the target. This is of interest as some recent studies point exactly towards this dose range in the context of secondary primary malignancies due to radiotherapy [3].

Putting aside any economic constraints, our current results indicate that antiprotons could be a serious contender for radiotherapy of specific tumor incidents. More work is needed to fully understand the biological effects outside the primary target as well as the tumor control possibility under different conditions. To identify those cases that would show a true benefit of antiprotons compared to protons or heavy ions biological models need to be modified to incorporate the complex radiation field generated by antiproton annihilations. For this more data on cell survival, DNA damage, and the effect of oxygen enhancement ratios (OER) will be needed from carefully designed benchmark experiments. These data can then be linked to the large body of biological data available in the literature from proton, carbon ion, pion, and neutron therapy

studies. Only then a final assessment of antiproton cancer therapy can be completed.

Our work is directly linked to the development and advancement of carbon ion therapy and we are closely collaborating with several groups active in this field. While we benefit significantly from the work on biological modeling and detector response to complex radiation fields, many of our technological developments will equally benefit the advancement of heavy ion therapy.

I. Introduction

The overall goal of the AD-4 Experiment is to study the biological effect of antiprotons in order to validate earlier theoretical predictions that antiprotons could produce a better therapeutic ratio for the treatment of well defined tumors. This prediction is based on two observations:

1. The physical dose should be augmented near the end of range due to the additional energy deposited locally when antiprotons annihilate.
2. Some of the additional energy deposited results from low energy heavy ion recoils produced in the annihilation event, which are expected to exhibit a higher biological efficiency.

To quantify these observations several studies are needed. One is a detailed measurement of the dose deposition of an antiproton beam of a specific energy entering a biological target, which then can be compared to Monte Carlo calculations and can be used to benchmark different available codes. The second piece of information needed is the relative biological effect with respect to a standard radiation type (typically a ^{60}Co source) along the path of the antiproton beam, preferably for a number of different cell lines extensively used in cancer research. Once these two questions are answered one can then use these results as input data for treatment planning tools and develop comparative treatment plans for a specific tumor for antiprotons, carbon ions, and protons. Based on these plans one can determine specific incidences of cancer where antiprotons could provide a significant benefit to patients.

Since antiproton annihilation also yields a significant component of medium and high-energy secondary particles, which will leave the annihilation vertex, a third, very critical issue to be studied is the biological effect of this background on cells outside the direct target area.

II. Clonogenic Survival of V79 Chinese Hamster Cells

Overview

In 2006, 2007, 2008, and 2009 we were assigned 1 week each of antiproton beam time, using a special extraction method providing a beam of 502 MeV/c antiprotons. As this extraction method is sufficiently different from normal AD operation it was decided to lump all beam time into a single run of 7 days of 24 hours. Typically, the first two to three days of the week are needed for beam set-up and dosimetry studies. Only when the desired beam quality is achieved, the

biological measurements can be initiated. As cell viability in the gelatin medium used is limited to 48 – 72 hours, this has to be orchestrated precisely and we typically allow some extra time before the start of biological measurements which always was (in case that set-up of the beam was completed faster) used beneficially for physics studies of dosimetry systems, beam monitors, and to collect dose data for Monte Carlo benchmarking.

The 502 MeV/c antiproton beam from the AD provides a penetration into our target of approximately 10 cm. We use a set of passive degraders to generate a spread-out Bragg peak of 10 mm depth, irradiating a volume of approximately 300 mm^3. This is much more closely resembling possible therapeutic situations encountered in realistic treatment scenarios than what was possible with the 300 MeV/c beam available before 2006. It also allows a much clearer separation between the entrance channel, where we expect low LET (and thereby low RBE) to dominate from the high LET/RBE region around the end of range. A typical dose-depth profile for antiprotons as obtained from FLUKA is shown in figure 1.

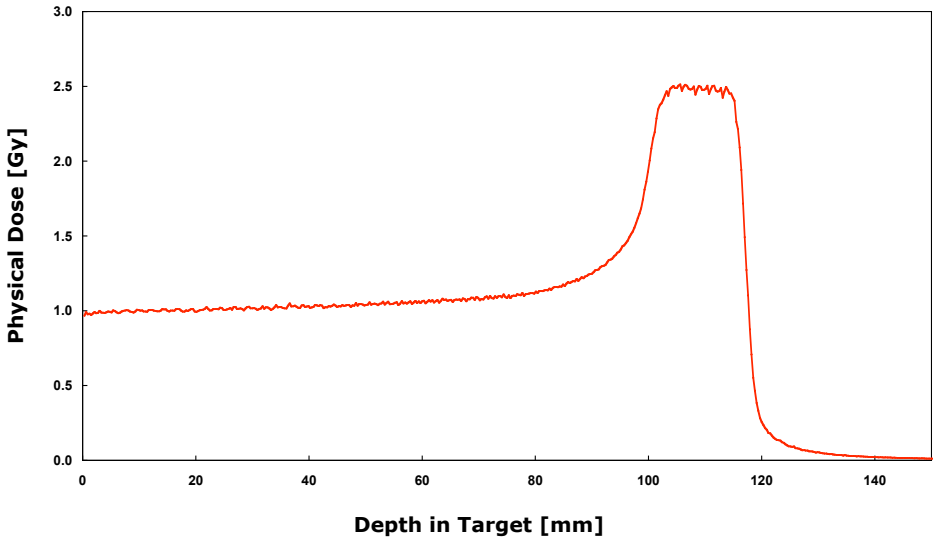

Fig. 1: Typical depth dose profile for antiprotons obtained from FLUKA (normalized to 1 Gy plateau dose).

In addition to the antiproton experiments at CERN we performed a comparison measurement using carbon ions at the heavy ion therapy unit at GSI in Darmstadt, Germany and a number of low LET calibration measurements needed for RBE analysis, which were performed at the German Cancer Research Center or at the Aarhus University Hospital. For the carbon ion measurements a spread-out Bragg Peak identical to the one shown above for antiprotons was programmed into the beam delivery software of the GSI treatment system.

Carbon Ion Measurements

In order to compare our studies with antiprotons to the gold standard of high LET particle therapy an experiment using carbon ions was conducted in early 2007 at GSI. Here a beam of clinical quality and absolute dosimetry was available and irradiations of 8 samples with plateau dose values between 0.3 and 4.0 Gy were performed. Survival data vs. depth are shown in figure 2.

Figure 3 shows the results of our analysis for the carbon ion experiment. Defining the plateau as data points 1 and 2 and the peak as points 9 – 14 of the depth survival curve (figure 2) we can plot survival vs. absolute dose for peak and plateau. In addition we plot survival vs. dose for a reference X-ray source with low LET and a RBE of 1. Using a biological endpoint of a survival rate of 10% we extract the $RBE_{0.1}$ for carbon ions as 1.38 in the plateau and 2.17 in the peak.

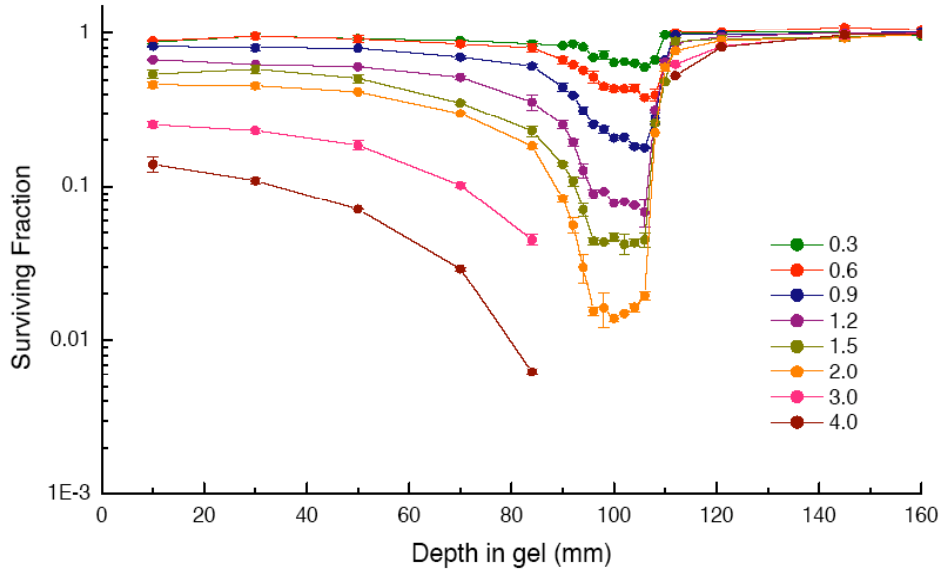

Figure 2: Survival fraction vs. depth in the target for V79 Chinese Hamster cells irradiated with carbon ions

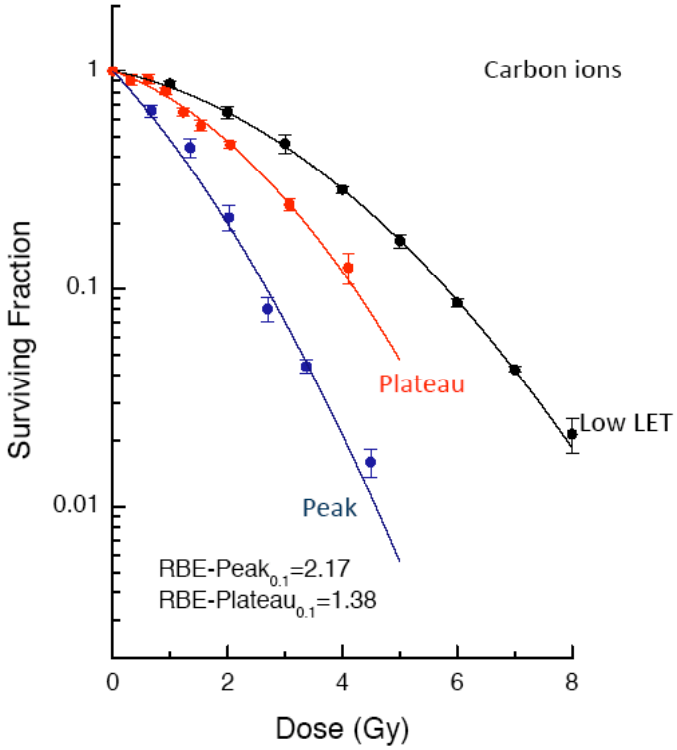

Figure 3: Survival fraction vs. absolute dose for V79 Chinese Hamster cells irradiated with carbon ions. By comparing the dose needed to achieve a survival of 10% using low LET X-rays to the dose needed when using carbon ions we extract a relative biological efficiency of 1.38 in the plateau and 2.17 in the peak.

Antiproton Measurements – V79 Chinese Hamster Cells

In 2006 we performed 4 different irradiations with nominal dose values of 0.25, 0.5, 1, and 5 Gy. Due to high uncertainties in estimating the absolute dose, only the lowest three dose values yielded useful data. For the 2007 run period we had improved our dosimetry capabilities and were able to control the absolute dose delivered to the target to within 10%, allowing us to augment above data sets. We performed irradiations on V79 cells for 6 different dose values. These dose values were selected using FLUKA based on dosimetric information obtained before the irradiation together with a best guess for the dose response curve based on previous measurements to achieve specific desired survival values in the peak and/or plateau region. Dosimetric control measurements between different badges were performed to assure the stability of the beam delivery system. The raw data obtained in 2007 are shown in figure 4 below. A final problem apparent from these data is the fact that we still failed to produce a flat response to the radiation within the spread-out Bragg peak. This was essentially due to the fact that we used pre-calculated kernels for the depth dose curve, which then were shifted according to additional degrader thickness, a method widely used in radiotherapy planning. This does not include the effect of additional lateral scattering, which dilutes the beam intensities for thicker degrader settings and a full Monte Carlo calculation was necessary to overcome this problem. (Note: this

problem is specific to the beam conditions here as the beam is too narrow to provide particle equilibrium at any arbitrary point in the target).

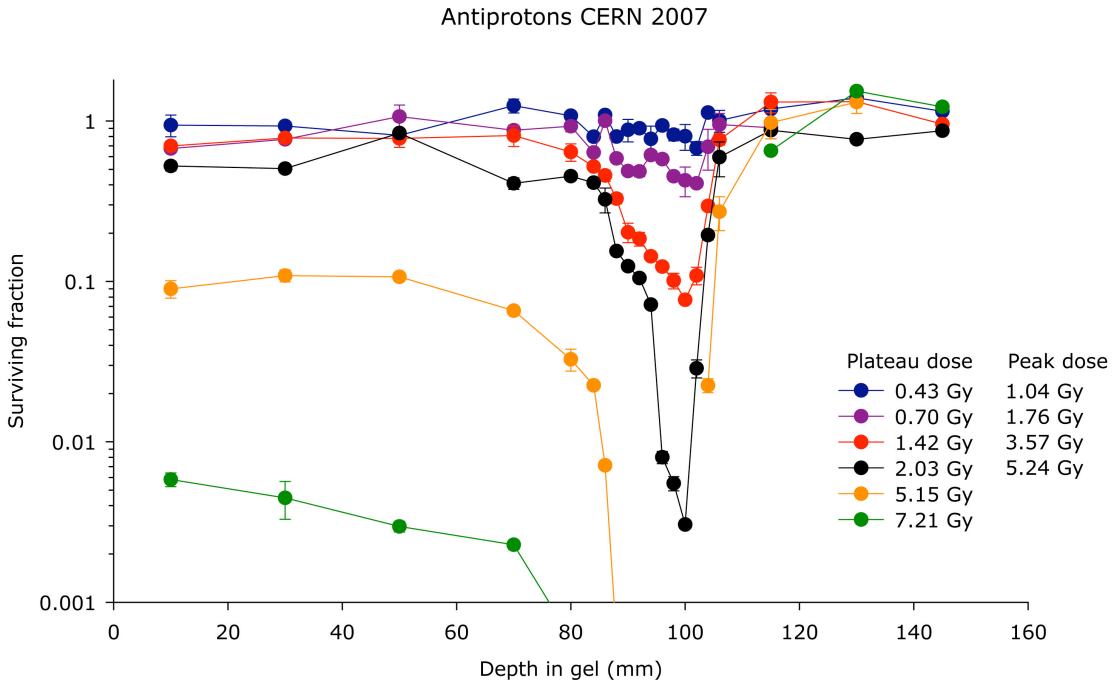

Fig. 4: Survival fraction vs. depth in the target for V79 Chinese Hamster cells irradiated with antiprotons. The dose values for the individual runs were estimated from FLUKA calculations using the number of antiprotons delivered and the radial beam profile obtained from radiochromic film irradiated simultaneously with the cell samples and analyzed after the run.

Figure 5 shows the raw data from the October 2008 data run where we achieve a Spread-Out Bragg Peak with a flat peak region. Also, the sensitivity of the clonogenic assay could be further improved and we are now able to measure survival fractions as low as 1 x 10^{-4}.

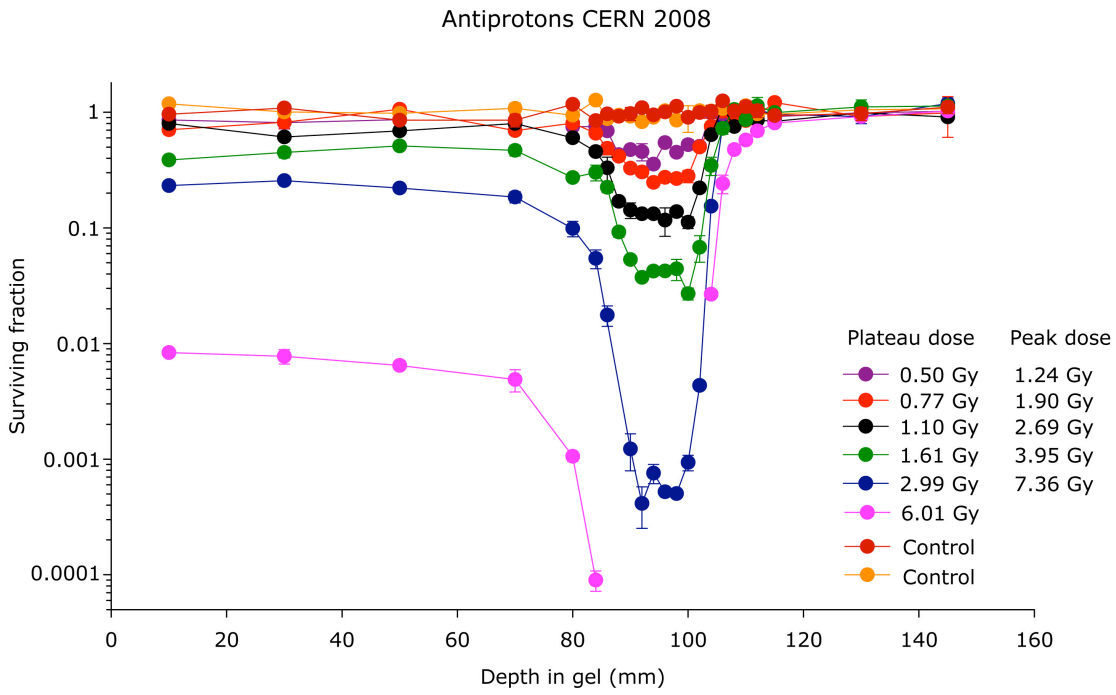

Fig. 5: Survival fraction vs. depth in the target for V79 Chinese Hamster cells irradiated with antiprotons during the 2008 run period.

In 2009 we continued these measurements with a focus on obtaining statistically significant data distal to the Bragg peak. After taking a few low dose runs to establish the exact position of the survival curve we then took long irradiation periods to achieve plateau doses of nominally 18 and 23.5 Gy. But even at these high dose levels the survival returned to values of 50% and higher 2 mm past the distal edge of the Bragg peak (100 mm). The slice at 102 mm is the only one yielding a large enough data spread to achieve a realistic fit of the linear-quadratic dose response curve to the data. From this one fit we conclude that the RBE is already returning towards the plateau value. We are currently working on implementing a more robust fitting routine including constraints on the parameters alpha and beta of the linear quadratic model commonly used to describe the survival vs. dose response, and allowing to make the plating efficiency (survival at dose equal to zero) a free parameter. This would allow to correct for slice-to-slice variation of cells being plated due to volume effects. Analysis of these data is ongoing and we therefore refrain from including data plots on the distal edge RBE in this report.

We used the data sets from 2007, 2008, and 2009 to analyse the dose response in the plateau region. Figure 6 shows the survival data from the three years together with a combined fit to all data and a dose response curve measured with ^{60}Co at Heidelberg after the 2008 run period. Using the dose values yielding a survival of 10% for both the fit to the data and the cobalt measurements we deduce a value for the $RBE_{plateau}$ = 1.25. While this value is well aligned with results of Monte Carlo studies performed by our group [9] the scatter of the data is still too large to quote this value as a final result.

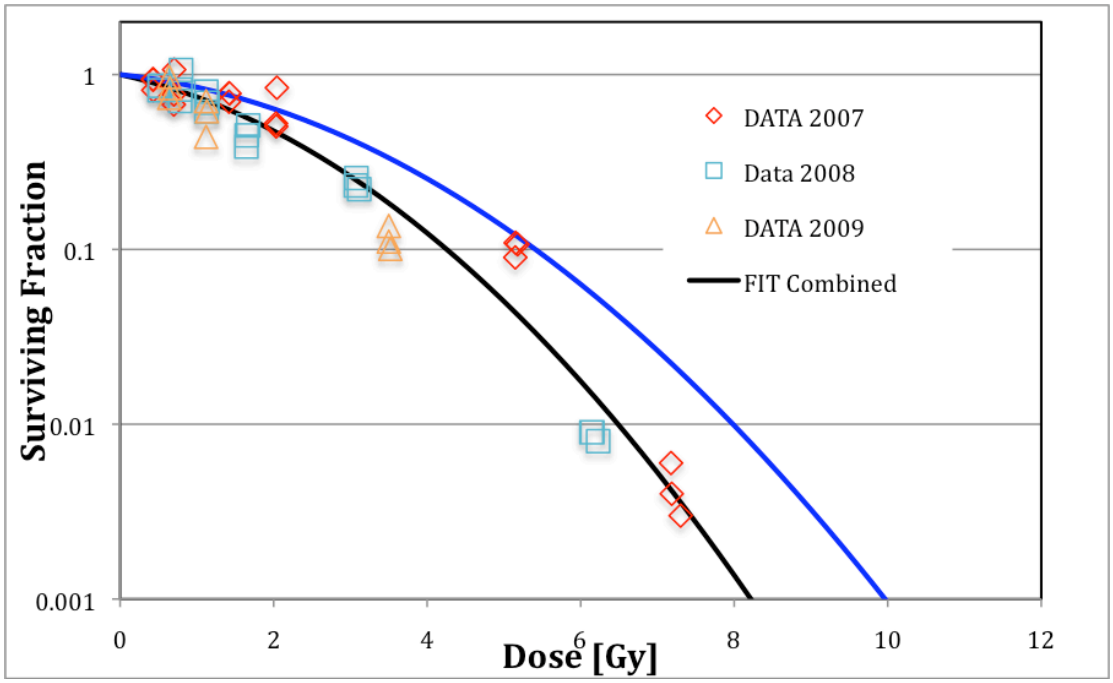

Fig. 6: Survival fraction vs. dose in the plateau region for V79 Chinese Hamster cells irradiated with antiprotons. For comparison the survival vs. dose for ^{60}Co irradiation is shown. From these results an RBE in the plateau for 10% clonogenic survival of 1.25 is obtained.

We are currently discussing changes to both the experimental protocol and the data fitting routine to improve this situation, but ultimately we need to experimentally establish error bars needed for proper weighting of the data in the fit. We also need more data points per slice as it is nearly impossible to fit 3 parameters to just 4 - 5 data points and place any level of confidence on the result. As the errors are not purely statistical but are due to variations in cell preparation, plating, and response it is established practice in radiotherapy to repeat experiments several times and then use the standard deviation of the entire sample as error bar. To do this we need to assure that we get survival data in independent experiments at the same dose point. For the plateau region this is relatively easy as small shifts in dose value can be corrected since the RBE in the plateau is constant. It is a much more difficult task in the peak region, where we superimpose Bragg peaks with different ranges, so that at each depth point a given dose value can consist of different mixtures of RBE values and therefore yield a different survival value for the same depth and dose point, dependent on the detailed set-up of the experiment. To achieve this we need to have a much more stringent control on beam intensity and position fluctuations in order to produce identical situations in independent experiments. This is the primary reason for us to develop a new beam monitoring system to allow shot to shot analysis of shape, intensity, and position of each extracted AD pulse (see section VI).

For illustration purposes only we show in figure 7 the dose response for the most distal position of the Bragg peak from 2008 in comparison to the plateau and cobalt data (for clarity we eliminated the individual data points in the plateau from the plot). The much reduced curvature of the survival curve is an indication for the increased LET and RBE in this region and the 10% survival extracted from this plot for $RBE_{10\%,peak}$ is 2.25, 1.8 times higher than for the plateau.

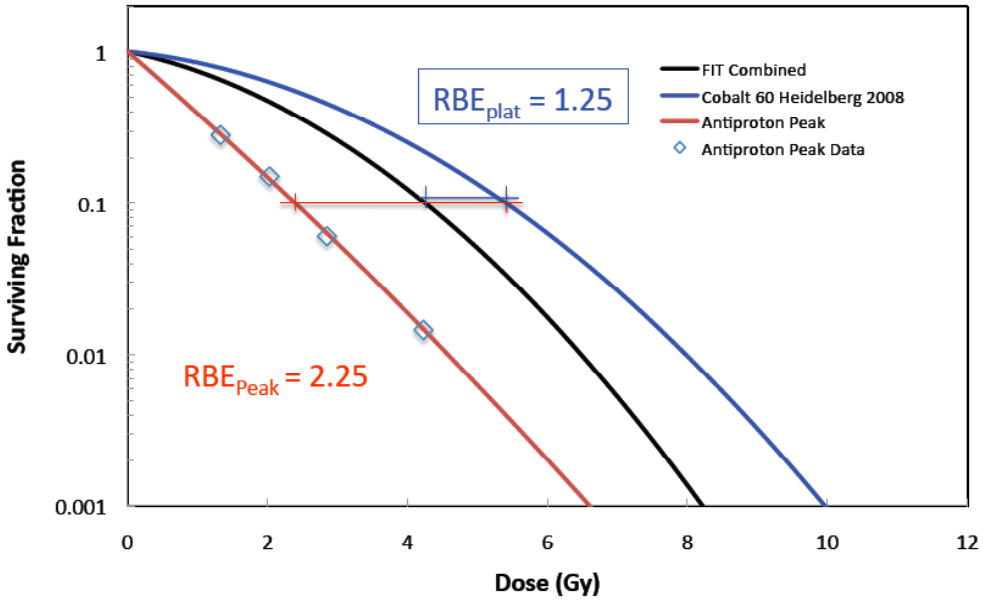

Fig. 7: Surviving fraction vs. dose for V-79 cells irradiated by 60Co, plateau antiprotons, and antiprotons in the distal edge of the Spread-Out Bragg Peak. RBE values quoted are for 10% clonogenic survival. The black and blue curves are identical to figure 6.

To illustrate the significance of these results we performed a Monte Carlo Study [10] where a 2 x 2 x 2 cm^3 target volume was irradiated with protons, carbon ions, and antiprotons. For each modality the constraint was set to the ICRU condition [11] that 95% of the target volume need to receive between 95% and 105% of the prescribed target dose. To achieve the best target coverage with the steepest dose gradient at the target boundary we individually optimized the incoming beams using lateral and energy weighting.

The results for both a single field and two opposing fields are shown in figure 8. Antiprotons have the highest peak to plateau ratio, as it is expected from the additional energy from the annihilation process. However, no dose is deposited by the protons beyond the SOBP in contrast to both antiprotons and carbon ions. In addition, the dose distribution outside the PTV is essentially of isotropic nature for antiprotons, whereas the carbon ions show a clear directional component, coming from secondary particles generated in-flight. While the dose distal to the Bragg peak initially is higher for antiprotons than for carbon ions, the dose tail for carbon ions extends further out and overtakes the antiproton tail a few centimeters past the distal edge.

A standard method to compare different modalities is to generate so-called dose-volume-histograms (DVH). Here the percentage of the volume of interest (VOI) receiving a specific dose level is plotted against the percentage of the target dose. For the prescribed target volume (PTV) this ideally should be a square function with 100% dose to 100% of the target volume and then a sudden drop to 0.

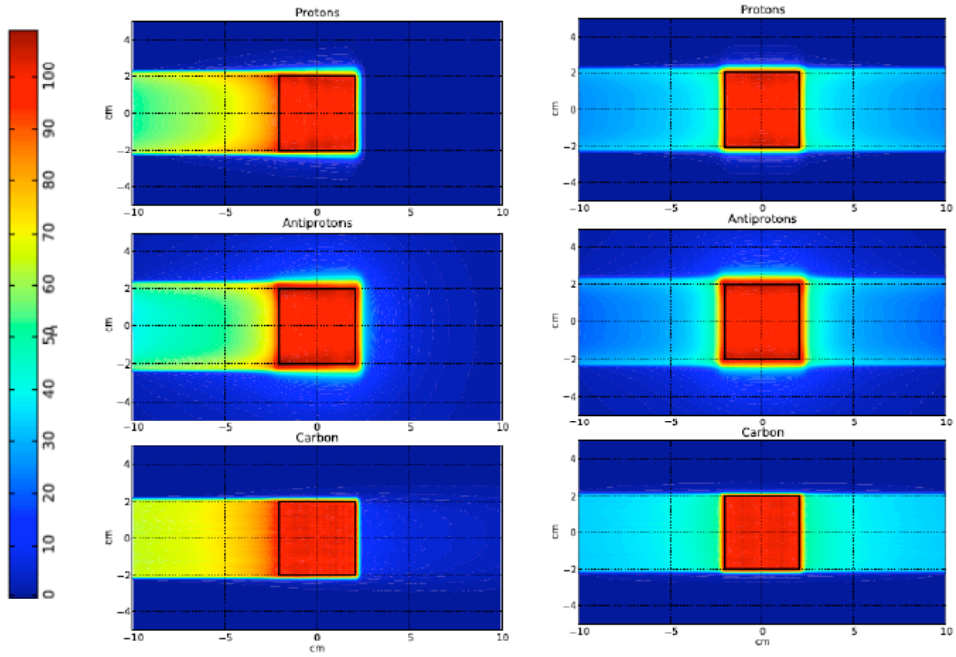

Fig. 8: Optimized single and double field dose plans for protons, antiprotons, and carbon ions. Antiprotons present the lowest dose in the entrance channel, but only at the expense of an extended low dose halo.

Figure 9 shows the DVH's for the PTV, and the lateral, proximal, and distal VOI's for a single field irradiation. To highlight the effect of the change in relative biological efficiency (RBE) between plateau and peak for antiprotons and carbon ions compared to protons, we did apply a hypothetical RBE ratio of 2 between the PTV and the region outside the PTV for both carbon ions and antiprotons. For the proximal region both carbon ions and antiprotons show clearly a superior behavior compared to protons, with antiprotons leading over carbon ions. But in the case of antiprotons this comes at the expense of an increased medium and low dose to the areas lateral and distal to the PTV. For laterally weighted beams the distal and lateral VOIs would be identical for antiprotons if lateral straggling of the beam could be ignored. The size of this effect can be deduced from the difference in the distal and lateral VOI for the case of protons. In regions lateral and distal to the PTV we find a larger volume receiving low dose (below 30% of the prescribed dose) for antiprotons than for carbon ions and protons.

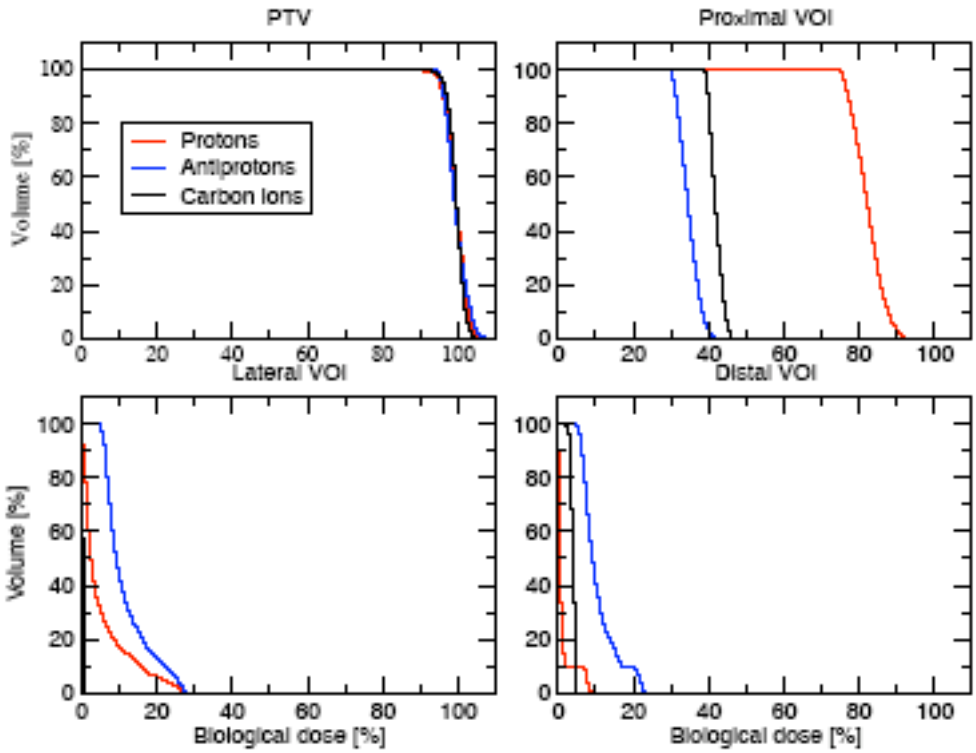

Fig. 9.: Biological dose-volume histograms for laterally optimized Fields, of the PTV and the 3 volumes of interest. Here a RBE ratio of 2 is assumed for antiprotons and Carbon ions, as described in the text.

To investigate the dose background outside the target volume, which is considered to be a relevant measure for the probability of long term complications, including second primary malignancy, we generate the DVHs for the entire phantom minus the PTV including a margin of 4 mm. In figure 10 we show the DVHs for the case of two opposing, laterally weighted fields, including again a hypothetical RBE ratio of 2 (right frame). We observe that antiprotons and carbon ions present a much lower radiation load to the whole body than protons in the high dose region, with a slight additional advantage for antiprotons over carbon ions for doses above approximately 15% of the prescribed target dose (in the RBE weighted case).

From our early observations on RBE the step function approach to RBE variation may be a good approximation in the case of antiprotons, but certainly is oversimplyfying the known RBE dependence vs. depth for carbon ions in favor of carbon ions. Future work will include more precise RBE vs. depth functions for both antiprotons and carbon ions.

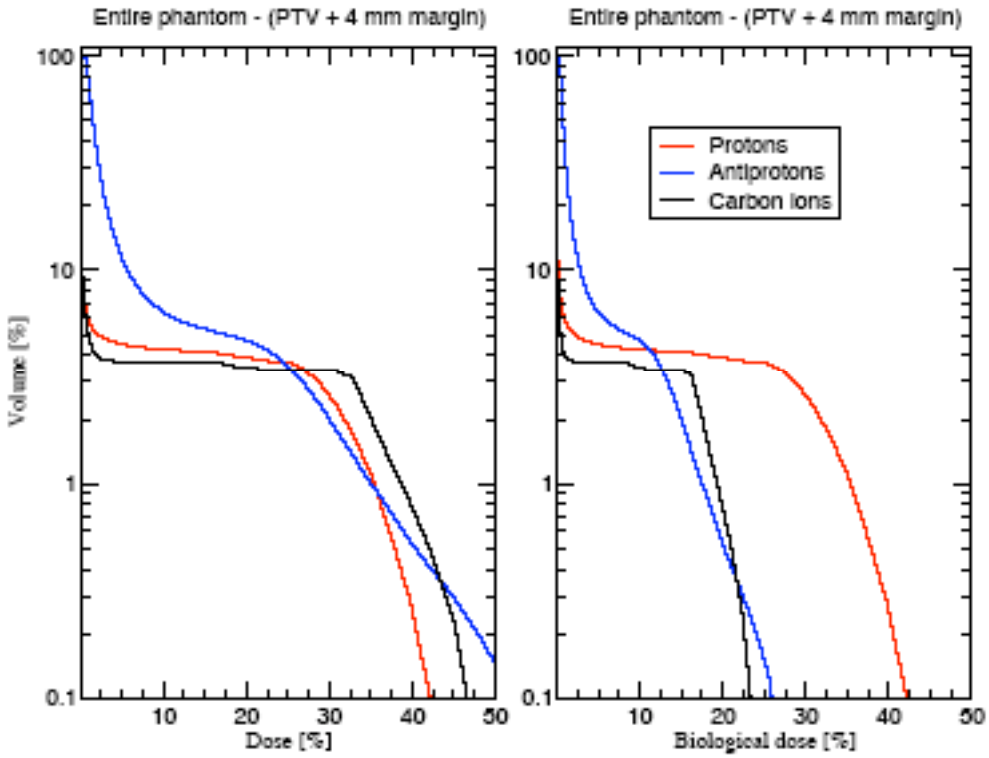

Fig. 10. DVH (left) and Biological-DVH (right) for the entire phantom minus the PTV and a 4 mm margin, using two opposing fields. For the Biological-DVH we assume a 2 times higher RBE in the PTV for antiprotons and carbon ions.

III. **Studies of cell damage in the peripheral region using γ-H2AX**

Introduction

In order to accurately investigate the implications of antiproton irradiation of living cells, it is important to analyze genetic complications that may arise in cells in regions peripheral to the targeted volume and may cause tumorigenesis and thus cancer development in previously healthy tissue. This would lead to the development of secondary primary malignancies, possibly many years after the treatment. To assess the risk of this necessitates developing experimental methods that allow sensitive and accurate measurements of critical DNA lesions.

Double strand DNA breaks (DSBs) are highly cytotoxic lesions which, if unrepaired or repaired incorrectly, can cause cell death or mutations in DNA of daughter cells [12]. As few as one DSB can cause cell death or genetic mutations leading to disregulation of cell growth and tumorigenesis.

Radiotherapy employs ionizing radiation (IR) to cause lethal damage to cells. It is widely accepted that cellular DNA is the most critical target. Immediately following an insult on DNA, damage sensing proteins (e.g. 53BP1, ATM) are recruited to the site of damage. This signals cell cycle arrest so that DNA repair can take place [13,14]. A key event in repair of a DSB is the phosphorylation of the histone H2AX necessary to unwind the DNA and allow repair proteins to access the DSB site.

The γ-H2AX is a very sensitive and specific immunocytochemical assay based on antibodies which recognize, and bind to, the phosphorylated H2AX histone as an accurate indicator of a DNA DSB. A secondary fluorescing antibody is then introduced to the cells which will bind to the primary antibody so the aggregate (or focus) around the DSB can be analyzed by fluorescence microscopy It has been shown [15] that there is an excellent 1:1 relationship between the number of γ-H2AX foci and the DSB induced. This assay is used frequently to investigate DNA damage induction by heat shock, chemotherapeutic agents, ionizing radiation, bystander signaling and other DNA damage agents.

In addition to direct damage from IR, there is mounting evidence for the existence of a non-targeted effect in which non-irradiated cells respond to the damage of their neighbours. This effect is known as the radiation induced bystander effect (RIBE) and it has been demonstrated in vitro for a number of endpoints including clonogenic survival, histone H2AX phosphorylation (γ-H2AX) and genetic instability. There are also a number of in vivo studies showing these effects in mice. It is likely that RIBEs may contribute to the clinical appearance of abscopal effects following radiotherapy [15-17].

The aim of our study is to quantify the individual contributions of antiproton annihilation, secondary dose (neutrons, pions etc), and bystander signalling caused in live cells exposed to an antiproton beam. The study has a particular focus on the impact outside of the target volume in terms of cell viability and genomic integrity. The γ-H2AX and micronucleus assays have been used to study immediate and longer term DNA damage respectively.

A pilot study at CERN in October 2008 demonstrated the applicability of this type of assay to studying antiproton induced DNA damage. These early experiments highlighted a number of issues: dose rate effects; contamination; the importance of cell culture facilities at or near CERN to obtain significant information from the samples (Problems highlighted in last year's report). Each of these issues has been addressed in the design of experiments for the 2009 beam time.

Antiproton irradiation

Slide flasks containing cell samples were mounted within a phantom in specially designed holders. These were positioned at depths of 20 mm (plateau) and 101 mm (centre of SOBP) (fig.11b). Cell samples were irradiated horizontally in an open water phantom with circulating water-glycerine mixture maintained at 4 ºC. Cells received estimated Bragg peak doses of 0.5, 0.75, 1.0, 2.0 and 5.0 Gy antiprotons.

In addition to irradiated samples there were three sets of unirradiated samples: 1) bystander cells (otherwise treated same as irradiated cells) were incubated at 37 ºC for 1 h with filtered media from SOBP directly irradiated sample, 2) cold controls which were otherwise treated the same as irradiated samples, 3) warm controls which remained incubating at 37 ºC in the lab and were fixed along with the other samples. This third set served as a control for the cold treatment of the cells.

a) b)

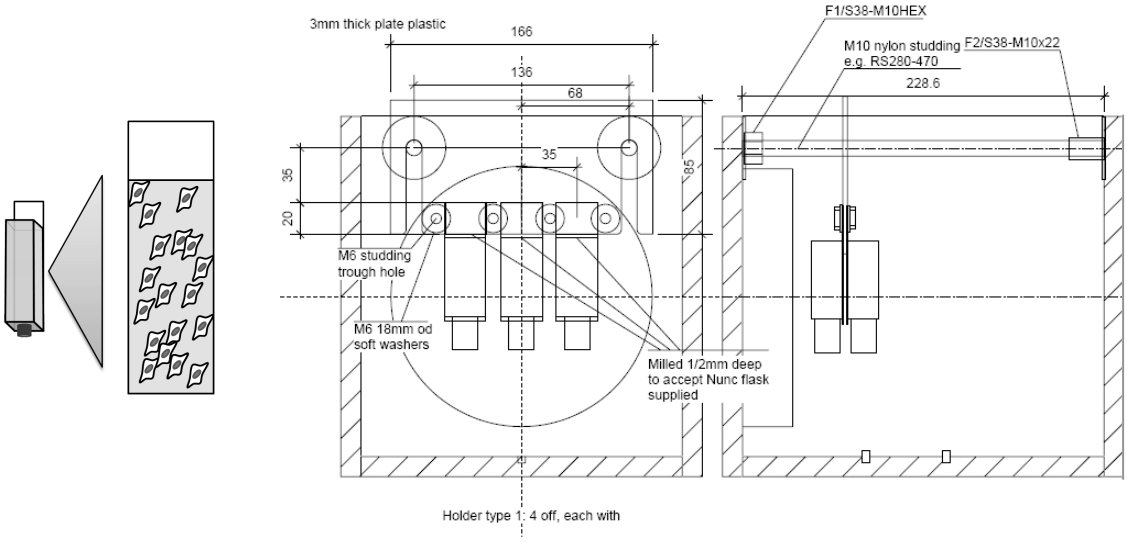

Fig.11. Experimental set-up for DNA damage experiments in 2009. Cells were seeded for radiation in polystyrene slide flasks (a) which were aligned and fixed in position (b) for irradiation with antiprotons. Schematic shows one sample holder as an example only. In the SOBP two flasks were fixed back-to-back as shown, cell monolayers separated by 3mm within the SOBP.

Results

Comparison of this year's controls with last year

Control samples displayed very low levels of DNA damage. Mean number foci from scoring of two independent samples of 200 cells was 1.7 as also measured under standard cell culture conditions in our laboratory in Belfast. Mean number foci per nucleus in the 2008 control was 13 (fig.12). Availability of sterile cell culture facilities, as well as the new experimental design for this year has ensured that not a single sample was contaminated despite being completely submerged in the water phantom for irradiations.

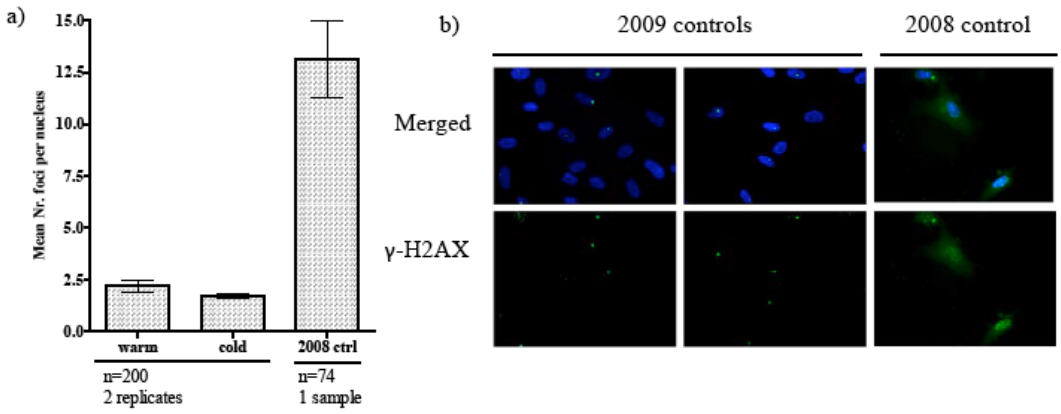

Fig.12. Non-irradiated control samples. (a) Foci score indicates level of endogenous DNA damage significantly decreased in control samples this year relative to last year's samples. Error bars also decreased substantially. Medians for warm and cold controls were not significantly different. Error bars indicate SEM. (b) Low levels of endogenous γ-H2AX foci in controls shown by immunofluorescence for 2009 samples.

Analysis of immediate DNA damage response to antiproton irradiation: γ-H2AX assay

Response to direct irradiation

Foci were scored in cells across the diameter of a 6mm spot on the sample slides which was positioned according to the gaf chromic film on each sample. All plateau samples contained many cells with bright and well defined foci. The mean number of foci in plateau samples was observed to be dose responsive. SOBP samples contained many cells which displayed very dense or clustered DNA double strand breaks (observed at x63 magnification) (fig.13b). Plateau samples did not show similar clustered foci regardless of dose or total number of foci (fig.13b). This indicates complex DNA damage caused by the antiproton annihilation. Number of foci per cell is also dose dependent in the SOBP. The experimental set up allowed two samples to be placed back to back (cell monolayers ~ 3mm apart) in the SOBP.

In addition to scoring the effects of direct irradiation, distant response perpendicular to the beam has also been recorded at 3mm increments away from the edge of the beam (assuming diameter of 6mm). At 3mm mean foci number drops dramatically and by 18mm the level of damage is similar to that in the controls (fig.13b). This trend will be analysed against the dose response measured by the gafchromic films.

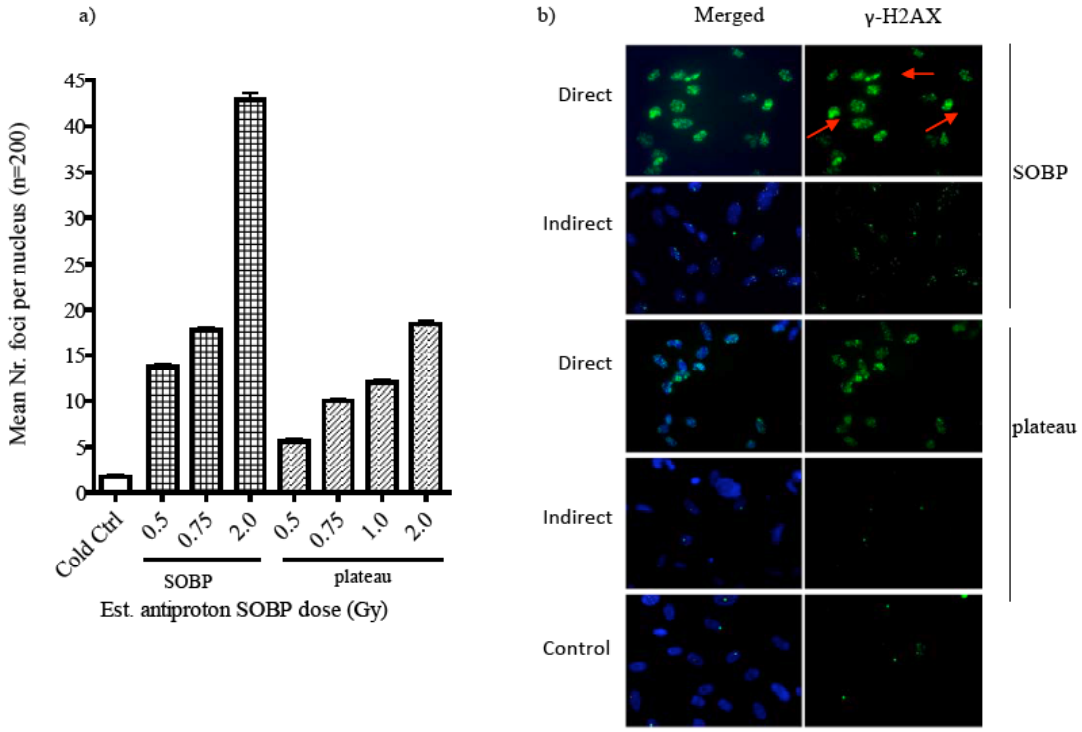

Fig.13. DNA damage dose response to antiproton SOBP and plateau. A) Mean number of foci per nucleus (200 nuclei per sample) increases with dose. B) Immunofluorescence images representative of foci distribution in 2Gy samples in SOBP and plateau. 'Direct' indicates cells that were placed in the beam path while 'Indirect' indicates cells within the same sample that were out of the beam path (not traversed by antiprotons). The mean foci number in these regions was similar to that of the control samples. Non-irradiated controls were otherwise treated same as irradiated samples. Red arrows indicate nuclei with clustered foci.

Indirect effects of antiproton irradiation

Scoring of γ-H2AX foci in bystander samples revealed a modest increase in DNA damage relative to the control samples. This effect does not, however, appear to be dose dependent. These cells were incubated with culture media from samples that were irradiated with antiprotons in the SOBP.

Analysis of secondary particle samples that were placed in the phantom at the time of irradiation and fixed adjacent to the directly irradiated samples display no significant increase in damage relative to the controls at this time. A strong response was not expected at the distances measured due to the relatively low dose of secondary particles, which drops off quickly with distance from the annihilation vertex. Only cells adjacent to the 2Gy sample gave a response that was significantly different to the controls. The data seem to indicate a dose dependent response; this will be confirmed with data from 5Gy samples, which have not yet been scored.

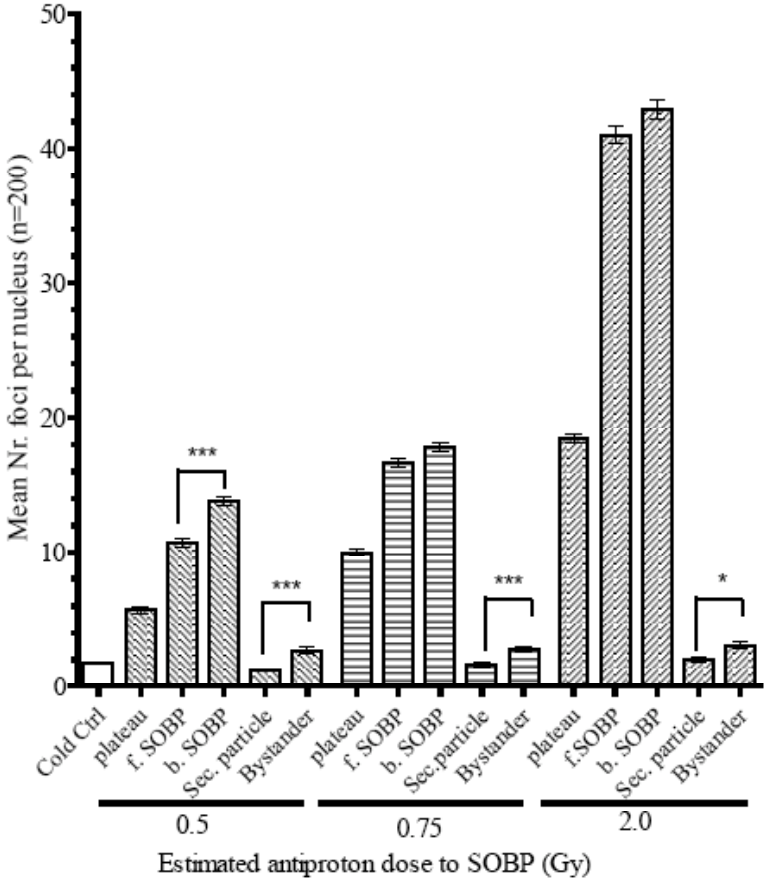

Fig.14. For each dose there are five sample sets for the γ-H2AX assay, each of which provides different information about the effects of either direct or indirect antiproton irradiation. Two sample were placed in the Bragg peak for each dose-labeled here as 'f.SOBP' and 'b.SOBP' (f: front, b: back) where f was the sample closer to the plateau. Mean foci number for f.SOBP and b.SOBP was only significantly different in the 0.5Gy dose samples, P<0.001). Results are for one experiment; error bars are SEM for 200 cells per sample. '***' indicates P value of less than 0.001, '*' indicates P value less than 0.05.

Analysis of longer term damage: Micronucleus assay

In non-irradiated control samples binucleated cells (BN) were counted within a sample spot of 6mm diameter. The percentage of BN in the control population was ~40%. Using this assay micronucleated cells (MN) are usually scored from 1000 BN. This was not possible here due to the small sampling radius.

Previous experiments using this assay for the AGO1522B cell line have demonstrated similar or lower binucleation in non-irradiated control samples. A repeat of these experiments with X-rays is planned following the same protocols as for antiproton experiments. Initial data suggests that the impact on cell survival is strongly linked to radiation quality.

The level of binucleation provides only information on the potential for cell survival. Of more importance for these experiments are those cells which survived antiproton irradiation and display evidence of genetic instability. Our data suggest that loss of genetic integrity is dose dependent for SOBP irradiation. Analysis of a

5Gy SOBP-irradiated sample is anticipated to show a complete loss of binucleation.

More interesting will be the MN induction in the plateau as there little cell killing is expected. Ultimately it will be the sub-lethal damage in the entrance channel that limits the outcome of any radiation treatment.

Future Experiments

1. Genetic instability

Up to now evidence from investigations into antiproton induced cell damage has indicated that exposed cells experience either lethal or non-lethal damage, where lethality is linked strongly to radiation LET. We are interested to know with what frequency there is genetic instability in cells that survive an antiproton dose.

It has been shown that antiproton traversal in the plateau dose result in elevated DNA damage and that impact for bystander signaling and secondary particles near the SOBP induces a level of damage above that of the control. Clonogenic survival data (at least in V79 cells) would indicate that damage expressed in the plateau region is non-lethal. The next question then is how successfully the non-lethal damage is repaired and at what rate genetic instability is created in the original cells and to what extent this is transmitted in their progeny.

2. Effectiveness of antiproton SOBP in hypoxic cells

It has been proposed that the high LET antiproton Bragg peak would potentially increase cell killing ability in hypoxic tissues. We would like to test this hypothesis in a cell model under hypoxia.

Note: A full report on the experiment is attached as Appendix II.

IV. Liquid Ionisation Chambers for LET Determination

1. Introduction

An important measure of the radiation quality for cancer therapy is the relative biological efficiency. Aside from a number of biological parameters like tissue type and cell environment amongst others, and physical parameters like dose and dose rate, RBE depends strongly on linear energy transfer (LET) or ionisation density. Weakly ionizing particles like x-rays have by definition an RBE value of 1. Protons are also considered weakly ionizing (except for the very distal edge of the Bragg peak) and typically, for clinical use, are assigned an RBE value of 1.1 throughout the entire path up to end of range. This is markedly different for heavy ions and antiprotons. Carbon ions, for example, are densely ionizing and have an RBE value that slowly increases from the entrance channel to the Bragg peak. In the case of antiprotons, our initial data indicate that the RBE value is close to the proton value along the main portion of the flight path in the target up to the very beginning of the Bragg peak with a relatively sudden increase to high RBE values at that point. For proper dose planning in heavy ion therapy and possible future use of antiprotons it is of great importance to gain more accurate knowledge of LET. The aim of our studies with the liquid ionization chambers (LICs) in the antiproton beam is to determine LET and ionization density along the beam path, and to compare these parameters with the results from protons and heavy ions. The ultimate goal is to develop general measurement methods and protocols to experimentally determine LET, which is closely related to RBE, at any given depth in the target.

The most commonly used detector for precision dosimetry in clinical beams is the air filled ionization chamber. Their use is simple and methods for dosimetry have been developed over several decades and are now generally summarized in so called "dosimetry protocols" [17].

Ionization chambers having a liquid rather than air as their sensitive media offer some advantages in dosimetry. These advantages include high sensitivity which allows the chambers to be manufactured with small geometrical dimensions, making them suitable for measurements in beams with steep gradients. The high sensitivity is also a clear advantage in beams with low dose rate. In addition, it is known that commonly used liquid ionization chambers have minimal field perturbing effects [18].

These advantages come at the cost of some drawbacks, such as leakage current and dependency on radiation quality and dose rate. The leakage current is not a serious drawback in clinical accelerator beams due to the high output from accelerators, but may be disturbing in low dose rate applications.

The dose rate dependence in the liquid ionization chamber response is caused by general recombination losses, in which case ions created by different incoming ionizing particles interact within the liquid volume and the net charge of the interacting species is reduced.

In addition to general recombination processes, initial recombination in liquid ionization chambers is substantial. The high degree of recombination losses, both general and initial, is caused by the relatively high density of the liquid (at least when compared to air) resulting in high ionization density in the liquid. This in combination with low ion mobility results in a pronounced recombination.

Initial recombination, i.e. when ions created by the same incident ionizing particle recombine, is clearly dependent on the ionization density along the incident particle. This process is often also referred to as columnar recombination. This means that initial recombination is a measure of the energy transferred "locally" from the incident particle to the medium. This offers the possibility to relate the initial recombination losses to the Linear Energy Transfer (LET) of the beam. The aim of the present measurements with liquid ionization chambers (LICs) in the antiproton beam is precisely this; to study initial recombination losses and relate it to LET.

2. Materials

Two new liquid ionization chambers from PTW, Germany, have been purchased for LET experiments. The chambers have identical radii of 1.25mm and electrode spacing of 0.35mm. One of the chambers was filled with a non-polar liquid, isooctane *(C_8H_{18}*, Merck, isooctane analysis grade, 99.5% purity) and the other chamber was filled with non-polar Tetramethylsilane (TMS, *$Si(CH_3)_4$*, Merck, NMR calibration grade, 99.7% purity). Both chambers are water tight.

The chambers were connected to a Keithley High Voltage Power supply, model 248, which is able to provide voltages up to 5000V. A Keithley 6517A programmable electrometer was used to read the charge collected from the ionization chambers. Both the power supply and the electrometer were controlled by a dedicated LabView program.

3. Methods

All measurements with the liquid ionization chambers were made in a water phantom. A large plane parallel air filled ionization chamber was mounted to the entrance of the phantom and used for monitoring shot-to-shot beam fluctuations [19].

3.1 Isooctane chamber

With the Isooctane chamber, measurements were made in the plateau region (10 mm depth), at the Bragg peak (100 mm depth) and at depths 2mm and 5mm beyond the distal edge of the Bragg peak. The applied voltages ranged from 100V up to 900V in steps of 100V and at each voltage 10 measurements were made. Occasionally, when measurements at a certain depth were repeated, the applied voltages ranged from 100V or 300V up to 900V in steps of 200V.

3.2 TMS chamber

With this chamber measurements were carried out in the plateau region and at the Bragg peak and at 2mm depth beyond the Bragg peak. The voltage range was the same as with the Isooctane chamber.

4. Summary of theory for columnar recombination

As mentioned in the Introduction, the aim of the liquid ionization chamber experiments is to determine the LET at different depths in water in the antiproton beam. This is done by studying columnar recombination losses in the chamber.

Jaffé [20] has developed a theory for columnar recombination and this theory is so far used in the present work. The theory is based on the assumption that the charge density (charge per unit volume) changes in the volume through diffusion and by recombination. According to Jaffé theory, the situation in liquids is

particularly simple since diffusion can be neglected in comparison with recombination losses [20,21].

The charge density change per unit time is therefore given by

$$\frac{\partial \rho}{\partial t} = -\frac{\alpha}{e}\rho^2 \qquad (1)$$

where ρ is the charge of one sign per unit volume, α the recombination coefficient and *e* the elementary charge.

Recombination losses can take place as long as ions of opposite sign occupy the same volume along an incident particle. The resulting recombination losses is easily shown to be

$$f_C = \frac{\rho}{\rho_0} = \frac{1}{u_C}\ln(1+u_C) \qquad (2)$$

with $u_C = \frac{(\alpha/e)}{(k_1+k_2)}\frac{\rho_0 h^2}{U}$, and where α is the recombination coefficient, and k_1 and k_2 are the mobilities of the positive and negative ions, ρ_0 is the initial charge per unit volume created by one proton, h is the thickness of the liquid layer (0.35mm) and U is the applied voltage.

Omitting the details of the calculations, the relative LET at depth z is determined from the relation

$$L_\phi(z) = \frac{Q_0(z)}{Q_0(z_0)}\frac{\phi(z_0)}{\phi(z)}L_\phi(z_0) \qquad (3)$$

where $L_\phi(z)$ is the fluence averaged LET at the depth z in water in the antiproton beam, $Q_0(z)$ the charge created per spill by the antiprotons and $\phi(z)$ is the antiproton fluence at the depth z in water. The reference depth, z_0, was taken at 10mm depth in water.

It is obvious that the LET values we are able to determine currently are relative ones. This, however, is not a serious drawback since the LET at the reference depth is easily calculated from stopping power values.

The fluence ratio, $\phi(z_0)/\phi(z)$, was calculated with the FLUKA Monte-Carlo code.

5. Correction for general recombination

Since the dose per spill is high in the antiproton beam, substantial general recombination losses are present in the liquid ionization chambers. The most widely used theory for correcting for general recombination loss is that due to Boag [22]. The theory's validity for liquid ionization chambers has been tested for dose per pulse in the range 0.06mGy/pulse up to 1.9mGy/pulse [18]. Since the dose per spill in the antiproton beam is much higher than the "clinical" values used by Johansson et al, a direct application of Boag's theory cannot be unquestionable and needs to be tested in more detail. It should be noted though, that using Boag's theory for our beam conditions led to excellent agreement

between measurements and Monte Carlo calculations for air filled ionization chambers [19].

6. Results and discussion

Figure 15 shows the results obtained with the Isooctane chamber. Using equation (3) for LET determination, the LET at the Bragg peak is calculated to be 9.0keV/µm. This value should be compared to 3.2keV/µm in the Bragg peak of a 173MeV proton beam determined with the same method. Kempe et al. [23] used the Monte-Carlo code Shield-HIT and calculated the fluence averaged LET in the Bragg peak to 3.63keV/µm in a 202MeV proton beam. The LET in the Bragg peak determined with the TMS chamber is 10.0keV/µm.

Since there is currently a high uncertainty in the correction for general recombination, definite conclusions about the fit to the Jaffé theory are difficult to make.

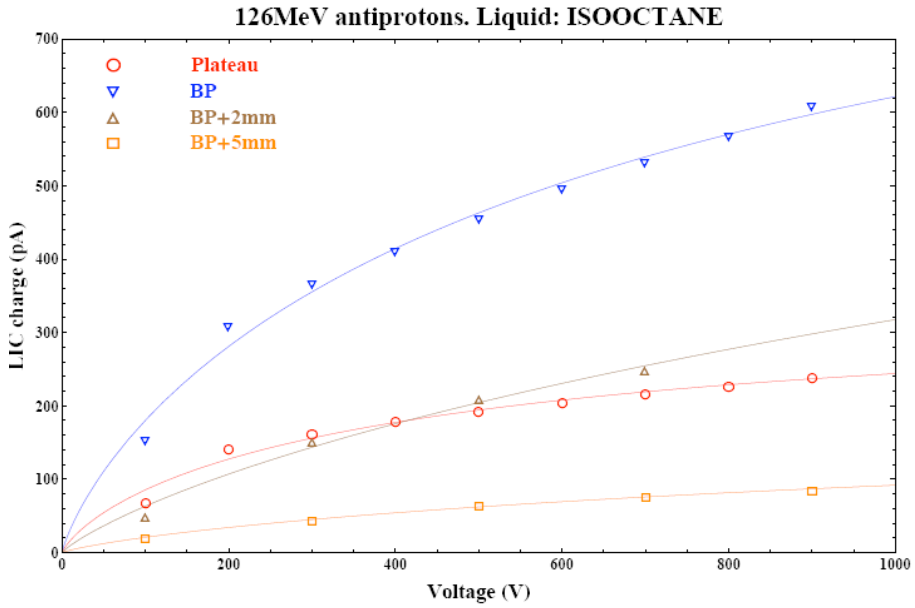

Figure 15. Charge measured at different applied voltage using a ionization chamber filled with Isooctane. The experimental values are fitted to the Jaffé theory.

7. Future work

The most important work to do in this subject is to determine the general recombination losses in a pulsed beam.

At the Dept. of Radiation Sciences, Radiation Physics, Umeå University, we are currently testing the Boag theory for liquid ionization chambers at high dose per pulse. The experiments are planned to be completed at the beginning of 2010. The experiments are done using a race-track microtron with a swept and pulsed beam. By stopping the sweep the dose per pulse is increased to much higher values than the values for which Boag's theory has been tested [18].

We expect that future experiments will cast some more light onto the validity of equation (3). The results presented in this section must therefore be considered as preliminary.

V. Real-time Imaging of the Antiproton Annihilation Distribution

Real real-time monitoring of the stopping distribution of particle beams used for radiotherapy provides the possibility of detecting possible errors in dose deposition early during a given treatment session, and may therefore help to improve the quality of the therapy. Imaging of 511 keV gammas from positron emitting isotopes generated in the target (in the case of proton therapy) or the beam (for carbon ions) have been studied for this purpose, and in-situ PET imaging for carbon ion therapy was an integral part of the therapy at GSI. Unfortunately, the lifetime of PET isotopes does not allow for a true real-time imaging and this method has been used mostly to confirm the correct dose delivery after a given treatment. Furthermore, there is no direct one-to-one relationship between the PET activity distribution and the dose distribution. More recently a development has been initiated to detect the prompt gammas from nuclear reactions with the target in proton therapy, which then can be correlated with the range distribution of primary particles.

Antiproton annihilation events produce several long-range secondary particles which can be detected in real time by standard high energy particle physics detector systems. We have performed Monte Carlo calculations [24] in order to study the feasibility of real-time imaging by detecting charged pions produced during antiproton irradiation of typical biological targets. A simple treatment plan in a water phantom is simulated and the results show that by detecting charged pions the position and the size of the planned target volume can be located with a precision on the order of 1-2 mm. Figure 16 shows the calculated dose distribution and differential antiproton fluence together with the vertex distribution detected with the virtual detector. The number of particles used in the calculation was 1 million, which is significantly less than 1% of the particles needed to deposit a 2 Gy fraction to the target volume.

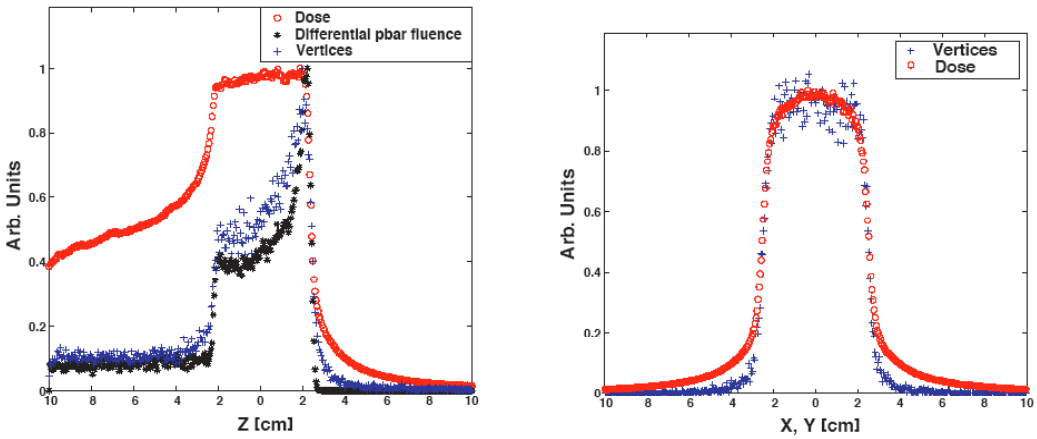

Fig. 16: Comparison of the physical dose (open circles) and the vertex position (crosses) along the beam axis (left panel) and perpendicular to the beam direction (right panel). In the left panel we also show the differential antiproton fluence.

To realize such a detection system with a minimal requirement on detection equipment we proposed, and performed first tests, of a novel arrangement. Instead of several layers of large size silicon pixel detectors facing the expected vertex distribution we propose to use a single area pixel detector rotated by 90 degrees, facing the vertex distribution edge on. This would lead to grazing incidence of particles from the annihilation vertex, leaving long tracks spanning several neighboring pixels. To test this concept we collaborated with the Petra Riedler and her colleagues from the ALICE Silicon Pixel Detector team from whom we were provided with one (spare) ladder consisting of 10 chips from the Alice detector, including control and read-out electronics. The detector is 13.6 cm long, 1.3 cm wide and 200 μm thick and consists of 320 columns of 425 μm width and 256 rows of 50 μm height, giving a total of approximately 82,000 pixels (figure 17).

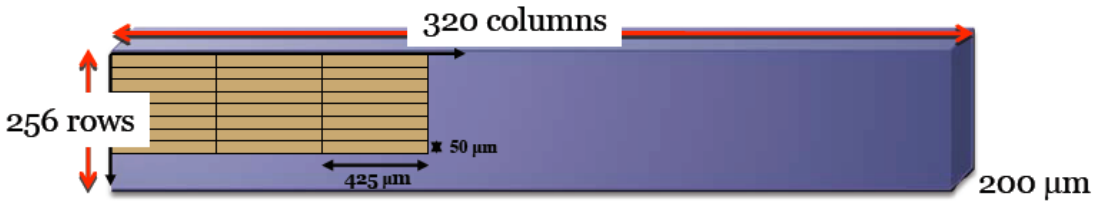

Fig. 17: Layout of the ALICE pixel detector used for the real-time imaging tests

For our tests we set up the detector with the 13 cm x 200 μm area facing the expected Bragg peak location (see figure 18). To cope with the high instantaneous annihilation rate of 3 x 10^7 antiproton annihilation in a 500 ns pulse the distance between the detector and the beam axis was chosen at 1.5 meters.

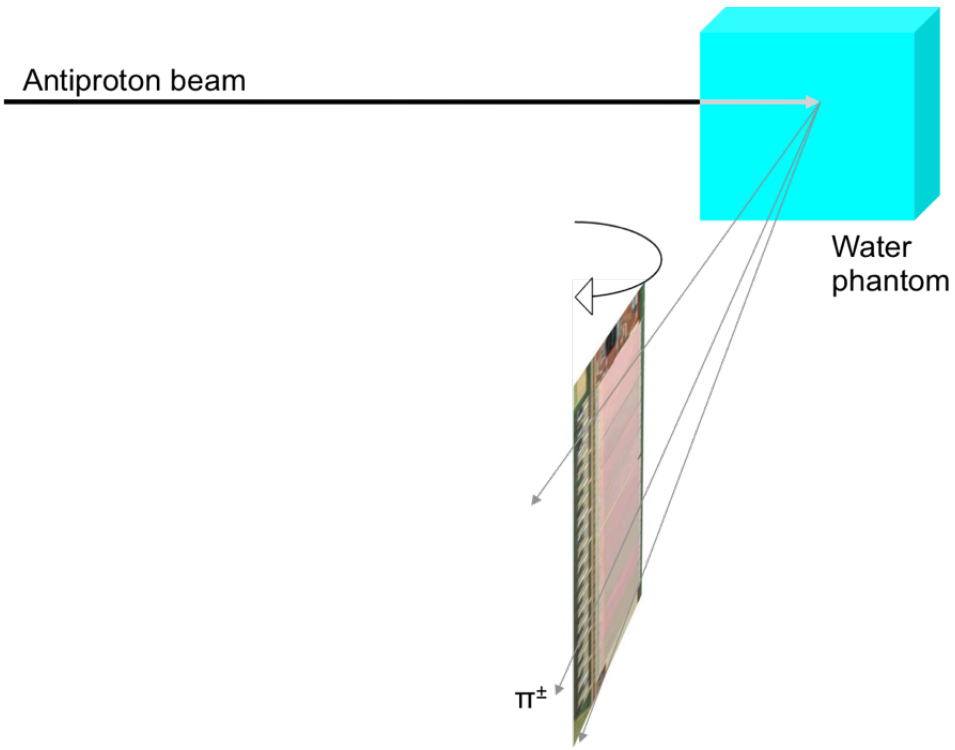

Fig 18: Arrangement of detector for real-time imaging tests at AD-4

When rotating the detector in ½ degree steps we can sweep across the spread-out Bragg peak and detect a change in track length distribution (figure 19).

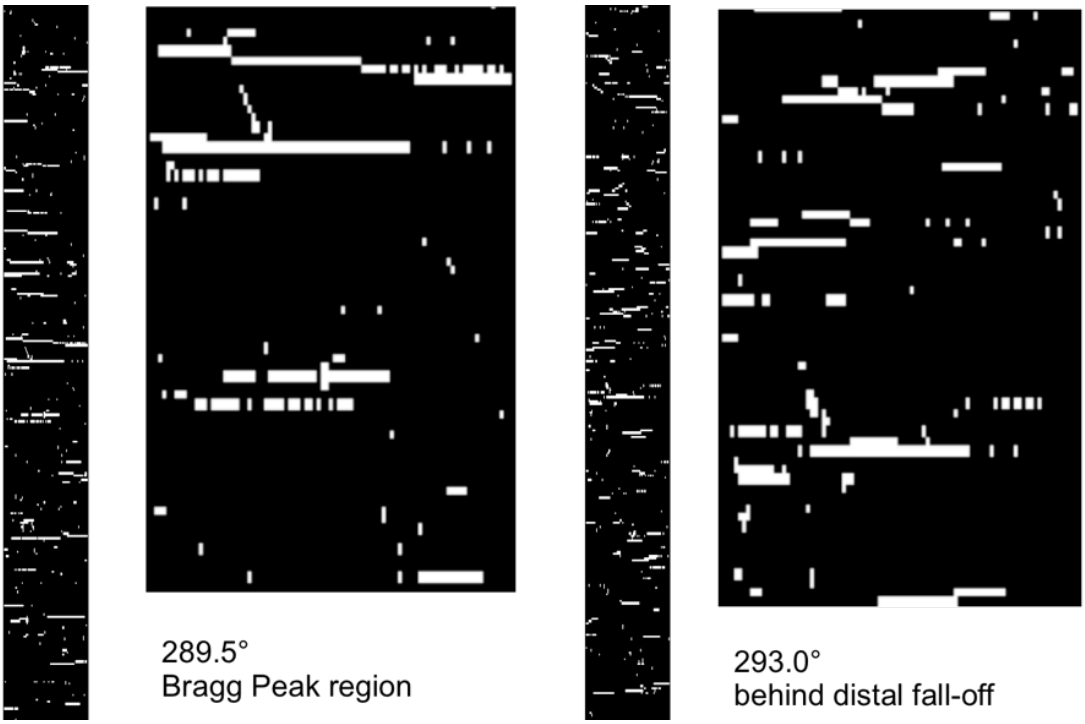

Fig. 19: Tracks detected from a single antiproton shot stopping in a water phantom 1.5 meters away from the detector. Shown are both the full detector ladder and a partial zoom to a smaller area. One can clearly see a difference in track length distribution for the two cases shown; left: facing at the Bragg peak, right: pointing towards the distal region.

We are currently in the process of optimizing a track recognition algorithm to automatically detect tracks as well as their direction and length. We also have set up the detector, phantom, and antiproton beam in FLUKA and are studying the optimal positioning of the detector with respect to the beam direction in terms of spatial resolution. Based on these results we plan to perform one additional data run from which we then will construct the axial distribution of annihilation vertices as a proof of principle of the method.

VI. Beam Monitor for Particle Therapy Application

In particle therapy in general and in our experiment in particular there is a strong need for a fast, high precision, 2 dimensional, well characterized beam monitor. Up to now we have used a fast transformer beam current monitor (BCM) from Bergoz Instrumentation to determine the integrated intensity for a single pulse. For the lateral position and shape of the beam pulse we use as a standard means Gafchromic Films, which have been widely used in particle beam therapy, as well as a scintillating screen, imaged with an intensified CCD camera. The films are used to integrate the overall exposure for a given irradiation period, but can not be used for single shot monitoring. The scintillator-camera combination was yielding good results at 50 MeV, but since the energy deposition of the 126 MeV beam is lower, the intensity is no longer sufficient to obtain a high resolution image from a single pulse.

We have therefore started a collaboration with the group of M. Caccia from the University of Insubria in Como to test the Mimotera Detector for our application. Mimotera is a Monolithic Active Pixel Sensor (MAPS) consisting of an array of 112 x 122 pixels of 153 µm x 153 µm each. The pixel arrays are subdivided into two interleaved sub-arrays, which are read out alternating to eliminate any dead time.

Initial tests performed during the 2009 beam time showed promising results and we are now developing a dedicated beam monitoring system for AD-4 based on the Mimotera design. Aside from using it as a beam position and beam shape monitor and as an alignment tool for the experiment we also will study the response of the detector to varying dose rate and LET in order to quantify the detector response for hadron therapy in general. In figure 20 we show a representative sample of images obtained from a single shot from the AD.

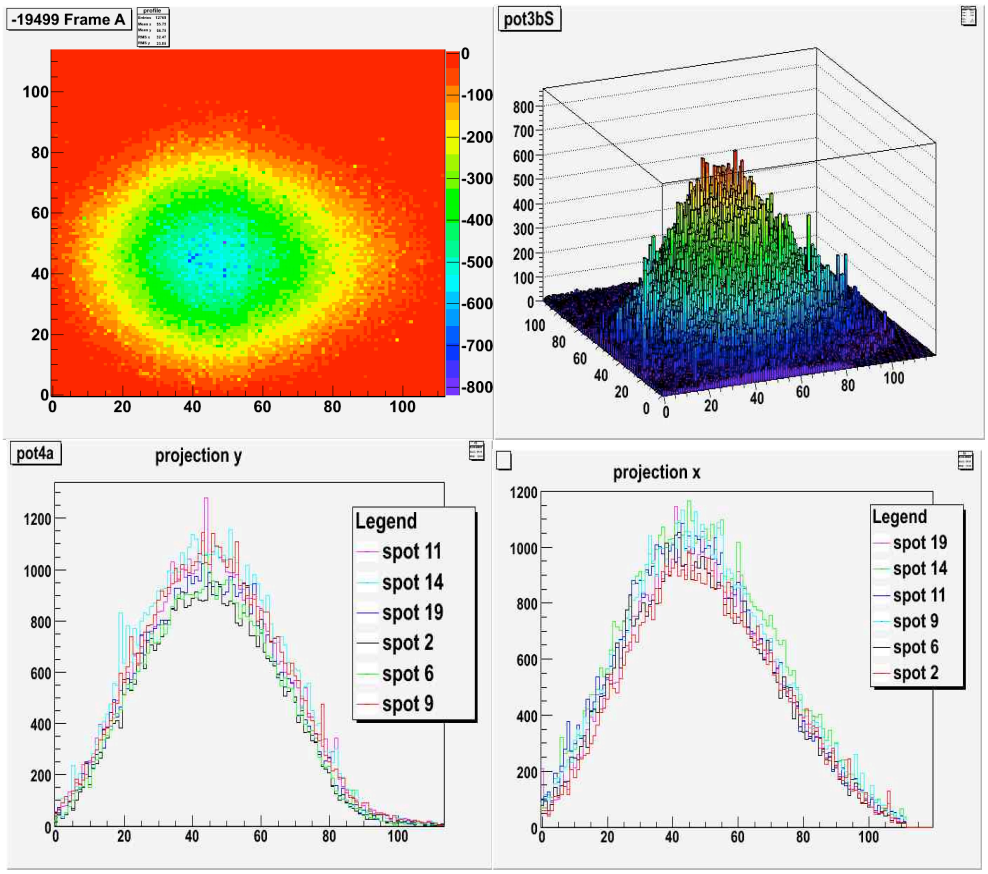

Fig. 20: Images from single antiproton shot. Clockwise from top left: 2D image of beam shape, 3D lego representation of beam intensity distribution, x and y radial distributions for 6 individual shots, showing small shot-to-shot variations.

VI. Summary, Outlook, and Beam Time

Using a total of less than six weeks of beam time over the last 7 years we have now reached the point where we have developed reliable tools for physical dosimetry and beam delivery planning. This has allowed us to collect an initial data set on the relative biological efficiency (RBE) of antiprotons for the chosen endpoint of 10% clonogenic survival of V-79 Chinese Hamster cells. Our current results are in agreement with the first measurements using a 50 MeV beam, where we measured a Biological Effective Dose Ratio (peak-to-plateau) four times larger for antiprotons than for protons. We observe a steep increase of RBE for antiprotons at the proximal edge of a spread-out Bragg peak (SOBP), in contrast to carbon ions, where RBE is increasing gradually along the beam path. Using a simplified model for RBE variation along the beam for both antiprotons and carbon ions, a step-function going from 1 to 2 only for the Bragg peak, we performed a dose planning study for a cubic target of 2x2x2 cm^3 dimension. Using the resulting dose volume histograms (DVH) we can identify certain advantages and disadvantages of the different particle modalities.

To quantify these findings and apply them to specific tumor incidents, believed to be prime candidates for a future antiproton therapy application, we have to confirm our current data and achieve a higher statistical significance by performing a number of independent repeat experiments. We also need to accumulate more data points for each depth slice in the target in order to obtain higher quality fits to the currently sparse data set. The dose planning studies need to be expanded by including the actual variation of RBE with depth for both carbon ions and antiprotons. And last-but-not-least, the optimization of the dose plan used for the different modalities needs to be improved.

In addition to RBE in the target area for clonogenic survival an equally, if not more important, question we have started to address is the effect of DNA damage and genetic mutation, and the relation to possible tumorigenesis. Such late effects are an active topic of discussions in all radiotherapy modalities and we expect more physical and biological studies in this field to become available in the next years.

As a support of these biological studies we have initiated developments on dosimetric tools for mixed radiation fields and have benchmarked our preferred Monte Carlo code (FLUKA) against experimental data. We have shown the possibilities for absolute dosimetry using Alanine pellets and linear energy transfer (LET) measurements using liquid ionization chambers. To improve our data taking capability at the AD we have identified novel beam monitors and are in the process of upgrading our experimental set-up.

One unique opportunity offered by antiprotons is the immediate, in principle particle-by-particle, detection of the annihilation vertex, and therefore dose distribution, in 3D. Monte Carlo studies have shown that a small percentage of the dose delivered during a treatment fraction would be sufficient to obtain a dose distribution confirmation within the range of a few percent. To experimentally realize this possibility we have performed first tests using one sample ladder of the ALICE silicon pixel detector. By setting it up in a geometry where secondary pions and gammas from the annihilation would have a grazing incidence, generating tracks across a large number of adjacent pixels, we have shown a dependency of track length on the angle between the detector orientation and the direction of incidence of the pions or gammas. We are now studying the

possibilities to expand this into a 3D reconstruction of vertex distribution with minimum detector requirements.

With the limited data set we have been able to accumulate in the few weeks of beam time since inception we have now reached a point where many of the initial questions have been addressed and a potential of a future use of antiprotons in cancer therapy can be argued. We now need to improve the statistical quality of the dataset to apply our knowledge to comparative dose planning exercises on specific, clinical relevant, tumor incidents.

To allow us to move forward in this research efficiently we request a continuation of the current procedure, where one week of AD beam time at 500 MeV/c is dedicated to our experiment. This week would be split between the continuation of clonogenic survival measurements, DNA damage studies, and the development of LET measurements with Liquid Ionization Chambers (LIC). Considering the 26 weeks of AD Physics time available in 2009, this is less than 5% of the total beam available, far less than the initial threshold of 10% discussed at the outset of AD-4. To set the amount of beam time in perspective: the overall number of antiprotons delivered to AD-4 since inception is equivalent to just a few hours of beam time at a carbon ion therapy facility.

To speed up progress and allow students to finish their thesis work in a timely manner we ask for 7 additional eight-hour shifts of 5 MeV beam into the AD-4 zone. This beam can be beneficially used for detector development, real time imaging studies, and tests of liquid ionization chambers and solid-state detectors in the high LET regime near the end of range. This would free up valuable beam time for the biological studies during the 500 MeV/c run week. Ideally we would prefer to have these low energy shifts bunched into one or two contiguous sessions.

VI. Acknowledgements

This work would not have been possible with out the support of the AD operation team. They have shown extreme motivation in providing the beam conditions needed for these measurements and have worked creatively in providing solutions to our needs without causing major interference with the main program of ultra-low energy antiproton physics of the AD community. We appreciate the help, support, and continued interest of many of our colleagues at the AD and many members of the CERN administrative, technical, and scientific staff.

The work was financially supported through many funding agency around the world, supporting the different institutions involved, as well as by special grants from the Danish Cancer Foundation and the European Union Marie-Curie Fellowship program.

References

1. Gray L, Kalogeropoulos TE.; Radiat Res. 1984;97:246–52.
2. Sullivan AH; Phys Med Biol 1985;30:1297–303.
3. Maurice Tubiana; Radiotherapy & Oncology 91: pp. 4-15 (2009)
4. Holzscheiter, MH et al.; Radiotherapy and Oncology 81 233–242 (2006)
5. A. Ferrari, P. R. Sala, A. Fasso, and J. Ranft, *"FLUKA: a multi-particle transport code"*, CERN-2005-10 (2005), INFN/TC 05/11, SLAC-R-773.
6. Kovacevic, S., Bassler, N., Hartley, O., Vranjes, S., Garaj-Vrhovac, V., Holzscheiter, M.; Int. J. of Rad. Biology 85: pp. 1148-1156 (2009)
7. Kantemiris, I., Angelopoulos, A., Bassler, N., Giokaris, N., Holzscheiter, M., Karaiskos, P., Kalogeropoulos, T.E.; Physics in Medicine and Biology, in print (2009)
8. Niels Bassler, Jan Alsner, Gerd Beyer, John J. DeMarco, Michael Doser, Dragan Hajdukovic, Oliver Hartley, Keisuke S. Iwamoto, Oliver Jäkel, Helge V. Knudsen, Sandra Kovacevic, Søren Pape Møller, Jens Overgaard, Jørgen B. Petersen, Timothy D. Solberg, Brita S. Sørensen, Sanja Vranjes, Bradly G. Wouters, Michael H. Holzscheiter; Radiotherapy and Oncology, **86** 14–19 (2008)
9. Niels Bassler, Michael Holzscheiter; Acta Oncologica 48: pp. 223-226 (2009)
10. International Commision on Radiation Units and Measurements. *Prescribing, recording, and reporting proton-beam therapy*. Technical Report 78, (2007)
11. K.K. Khanna, S.P. Jackson. *Nat. Genet.* **27** (2001) 247-254
12. Bryant, P.E. International Journal of Radiation Biology 48 (1985): 55-60
13. Rogakou, E. P., D. R. Pilch, A. H. Orr, V. S Ivanonva, and W. M. Bonner. The Journal of Biological Chemistry 273: pp. 5858-5868 (1998)
14. Mothersill, C., and Seymour, C.B. Radiation Research 149 (1998): 256-262.
15. Seymour, C. B., Carmel. Mothersill, C. Rad. Research 153 (2000): 508-511.
16. Mancuso, M, and et al. PNAS, USA 105 (2008): 12445-12450.
17. International Atomic Energy Agency (IAEA) 2000. Absorbed Dose Determination in External Beam Radiotherapy. An International Code of Practice for Dosimetry Based on Standards of Absorbed Dose to Water. IAEA Technical Reports Series (TRS) 398. IAEA, Vienna
18. Johansson B, Wickman G and Bahar-Gogani J; Phys. Med. Biol. 42: p. 1929 (1997)
19. Bassler, N., Holzscheiter, M., Jäkel, O., Knudsen, H., Kovacevic, S., AD-4/ACE Collaboration; Physics in Medicine and Biology 53: pp. 793-805 (2008)
20. Jaffé G, I; Ann. Phys. [4] 42 p. 303 (1934)
21. Kramers H A; Physica 18, p. 665 (1952)
22. Boag J W; Brit. J. Radiol, p. 649 (1952)
23. Kempe J, Gudowska I and Brahme A; Med. Phys. 34: pp. 183-192 (2007)
24. Kantemiris, I., Angelopoulos, A., Bassler, N., Giokaris, N., Holzscheiter, M., Karaiskos, P., Kalogeropoulos, T.E.; Physics in Medicine and Biology, in print (2009)

Appendix I

List of publications from the AD-4 Collaboration

1. J.N. Kavanagh, F.J. Currell, D.J. Timson, M.H. Holzscheiter, N. Bassler, R. Herrmann, G. Schettino; 'Induction of DNA Damage by Antiprotons for a Novel Radiotherapy Approach'; *submitted to European Physical Journal D* (2009)
2. Niels Bassler, Ioannis Kantemiris, Julia Engelke, Michael Holzscheiter, Jørgen B. Petersen, 'Comparison of Optimized Single and Multifield Irradiation Plans of Antiproton, Proton and Carbon Ion Beams', submitted to *Radiotherapy and Oncology* (2009)
3. Bassler, N., Holzscheiter, M.H., Petersen, J.B., Neutron Fluence in Antiproton Radiotherapy, Measurements and Simulations', submitted to *Physics in Medicine and Biology* (2009)
4. Kantemiris, I., Angelopoulos, A., Bassler, N., Giokaris, N., Holzscheiter, M., Karaiskos, P., Kalogeropoulos, T.E., 'Real-time imaging for dose evaluation during antiproton irradiation', *Physics in Medicine and Biology*, in print (2009)
5. Kovacevic, S., Bassler, N., Hartley, O., Vranjes, S., Garaj-Vrhovac, V., Holzscheiter, M., 'V-79 Chinese Hamster Cells irradiated with antiprotons, a study of peripheral damage due to medium and long range components of the annihilation radiation', *Int. J. of Rad. Biology* 85: pp. 1148-1156 (2009)
6. Fahimian, B.P., DeMarco, J.J., Keyes, R., Bassler, N., Iwamoto, K.S., Zankl, M., Holzscheiter, M.H., 'Antiproton radiotherapy: peripheral dose from secondary neutrons', *Hyperfine Interaction* 194: pp. 313-318 (2009)
7. Bassler, N., Holzscheiter, M. 2009, 'Calculated LET Spectrum from Antiproton Beams Stopping in Water', *Acta Oncologica* 48: pp. 223-226 (2009)
8. Niels Bassler, Jan Alsner, Gerd Beyer, John J. DeMarco, Michael Doser, Dragan Hajdukovic, Oliver Hartley, Keisuke S. Iwamoto, Oliver Jäkel, Helge V. Knudsen, Sandra Kovacevic, Søren Pape Møller, Jens Overgaard, Jørgen B. Petersen, Timothy D. Solberg, Brita S. Sørensen, Sanja Vranjes, Bradly G. Wouters, Michael H. Holzscheiter; 'Antiproton radiotherapy', *Radiotherapy and Oncology* 86: pp. 14-19 (2008)
9. Knudsen, H., Holzscheiter, M.H., Bassler, N., Alsner, J., Beyer, G., DeMarco, J.J., Doser, M., Hajdukovic, D., Hartley, O., Iwamoto, K.S., Jäkel, O., Kovacevic, S., Møller, S.P., Overgaard, J., Petersen, J.B.B., Ratib, O., Solberg, T.D., Vranjes, S., Wouters, B.G., the CERN ACE Collaboration, , 'Antiproton Therapy', *Nuclear Instruments and Methods in Physics Research B* 266: pp. 530-534 (2008)
10. Bassler, N., Holzscheiter, M., Jäkel, O., Knudsen, H., Kovacevic, S., AD-4/ACE Collaboration, 'The Antiproton Depth-Dose Curve in Water', *Physics in Medicine and Biology* 53: pp. 793-805 (2008)

11. Bassler, N., Hansen, J.W., Palmans, H., Holzscheiter, M.H., Kovacevic, S., 'The Antiproton Depth Dose Curve Measured with Alanine Detectors', *Nuclear Instruments and Methods in Physics Reseach B* 266: pp. 929-936 (2008)

12. Bassler, N., Knudsen, H., Møller, S.P., Petersen, J.B.B., Rahbek, D., Uggerhøj, U.I., 'Bubble detector measurements of a mixed radiation field from antiproton annihilation', *Nuclear Instruments and Methods in Physics Research B* 251: pp. 269-273 (2006)

13. Holzscheiter, M.H., Bassler, N., Agazaryan, N., Beyer, G., Blackmore, E., DeMarco, J.J., Doser, M., Durand, R.E., Hartley, O., Iwamoto, K.S., Knudsen, H., Landua, R., Maggiore, C., McBride, W.H., Møller, S.P., Petersen, J.B.B., Skarsgard, L.D., Smathers, J.B., Solberg, T.D., Uggerhøj, U.I., Vranjes, S., Withers, H.R., Wong, M., Wouters, B.G. 2006, 'The biological effectiveness of antiproton irradiation', *Radiotherapy & Oncology* 81: pp. 233-242 (2006)

14. Bassler, N., Holzscheiter, M.H., Knudsen, H., 'Cancer therapy with antiprotons', in *Low Energy Antiproton Physics-LEAP '05, AIP Conference Proceedings CP769*, pp. 423-430 (2005)

15. Holzscheiter, M.H., Agazaryan, N., Bassler, N., Beyer, G., DeMarco, J.J., Doser, M., Ichioka, T., Iwamoto, K.S., Knudsen, H., Landua, R., Maggiore, C., McBride, W.H., Møller, S.P., Petersen, J.B.B., Skarsgard, L.D., Smathers, J.B., Solberg, T.D., Uggerhøj, U.I., Withers, H.R., Vranjes, S., Wong, M., Wouters, B.G. 2004, 'Biological effectiveness of antiproton annihilation', *Nuclear Instruments and Methods in Physics Reseach B* 221: pp. 210-214 (2004)

16. Maggiore, C., Agazaryan, N., Bassler, N., Blackmore, E., Beyer, G., DeMarco, J.J., Doser, M., Gruhn, C.R., Holzscheiter, M.H., Ichioka, T., Iwamoto, K.S., Knudsen, H., Landua, R., McBride, W.H., Møller, S.P., Petersen, J.B.B., Smathers, J.B., Skarsgard, L.D., Solberg, T.D., Uggerhøj, U.I., Withers, H.R., Wouters, B.G., 'Biological Effectiveness of Antiproton Annihilation', *Nuclear Instruments and Methods in Physics Research B* 214: pp. 181-185 (2004)

Appendix II

Analysis of Antiproton induced DNA damage: non-targeted effects of radiation.
Queen's University of Belfast.

Introduction

Radiotherapy employs ionizing radiation (IR) to cause lethal damage to cells. It is widely accepted that cellular DNA is the most critical target. Immediately following an insult on DNA, damage sensing proteins (e.g. 53BP1, ATM) are recruited to the site of damage. This signals cell cycle arrest so that DNA repair can take place (Bryant, 1985; Bonner et al, 1998). If the damage is too extensive to be repaired programmed cell death (apoptosis) will be initiated. Damaged cells which are also deficient in cell cycle check point proteins may not arrest and enter mitosis. The result is mitotic catastrophe, a common phenotype of which is enlarged cells containing multiple micronuclei. Following a mitotic catastrophe, cells may continue to cycle for a short time but are not viable long term as they lack significant genetic information, and will ultimately undergo cell death. This type of damage-induced response, called mitotic cell death, can be a mechanism by which cells prevents aneuploidization which can lead to tumorigenesis (Castedo, 2004; Molz et al 1989).

In addition to direct damage from IR, there is mounting evidence for the existence of a non-targeted effect in which non-irradiated cells respond to the damage of their neighbours. This effect is know as the radiation induced bystander effect (RIBE) and it has been demonstrated in vitro for a number of endpoints including clonogenic survival, histone H2AX phosphorylation (γ-H2AX) and genetic instability. There are also a number of in vivo studies showing these effects in mice. It is likely that RIBEs may contribute to the clinical appearance of abscopal effects post radiotherapy (Mothersill,1998; Seymour,2000; Mancuso,2008).

The aim of this study was to quantify the individual contributions of antiproton annihilation, secondary dose (neutrons, pions etc) and bystander signalling caused in live cells exposed to an antiproton beam. The study has a particular focus on the impact outside of the target volume in terms of cell viability and genomic integrity. The γ-H2AX and micronucleus assays have been used to study immediate and longer term DNA damage respectively. A pilot study at CERN in October 2008 demonstrated the applicability of this type of assay to studying antiproton induced DNA damage. These early experiments highlighted a number of issues: dose rate effects; contamination; the importance of cell culture facilities at or near CERN to obtain significant information from the samples. (Problems highlighted in last year's report.) Each of these issues has been addressed in the design of experiments for the 2009 beam time. Significant changes were made to the experimental set-up to minimise possibility of leaking or infections in the cell culture. In addition Oliver Hartley, at Geneva Medical University opened his lab to our group so that tissue culture could be carried out under sterile conditions within a short time before each experiment. This helped minimizing stress due to external factors as confirmed by a normal background level of damage in controls. Finally, modifications to experimental design allowed us to compensate for effects of dose rate on the DNA damage assays used.

In addition to cell experiments, the plasmid DNA assay was revisited to trial an optimised protocol which has previously demonstrated increased sensitivity to clinically relevant radiation doses (Wyer et al 2009; Folkard, 1999).

Materials and Methods

Cell Culture

AGO1522 human fibroblast cells were cultured in filtered alpha-MEM (LONZA, BioWhittaker®) supplemented with foetal bovine serum (15%), penicillin (100 IU/ml) and streptomycin (100 µg/ml) and Hepes buffer (25 mM) in a 95% air/5%CO_2 37^{o}C atmosphere. 10 h prior to treatment, cells were detached from culture flasks and were seeded in polystyrene slide flasks (NUNC) in 2 ml alpha-MEM and incubated (fig.1a). For γ-H2AX assay ~6×10^5 cells seeded and for micronucleus assay ~ 3×10^4 cells seeded per sample. 2-3 h prior to irradiation sample flasks were filled with cold supplemented alpha-MEM (eliminating as much air as possible) and flasks were sealed closed. Samples transported to CERN in

insulated container maintaining temperature at ~4ºC. Cell samples were kept cold for a maximum of 12 h. MTT tests were preformed in Geneva to show this did not have significant effect on cell viability.

Antiproton irradiation

Slide flasks containing cell samples were mounted within a phantom in specially designed holders. These were positioned at depths of 20 mm (plateau) and 101 mm (centre of SOBP) (fig.1b). Cell samples were irradiated horizontally in an open water phantom with circulating water-glycerine mixture maintained at 4 ºC. Cells received estimated Bragg peak doses of 0.5, 0.75, 1.0, 2.0 and 5.0 Gy antiprotons. In addition to irradiated samples there were three sets of unirradiated samples: 1) bystander cells (otherwise treated same as irradiated cells) were incubated at 37 ºC for 1 h with filtered media from SOBP directly irradiated sample, 2) cold controls which were otherwise treated the same as irradiated samples, 3) warm controls which remained incubating at 37 ºC in the lab and were fixed along with the other samples. This third set served as a control for the cold treatment of the cells.

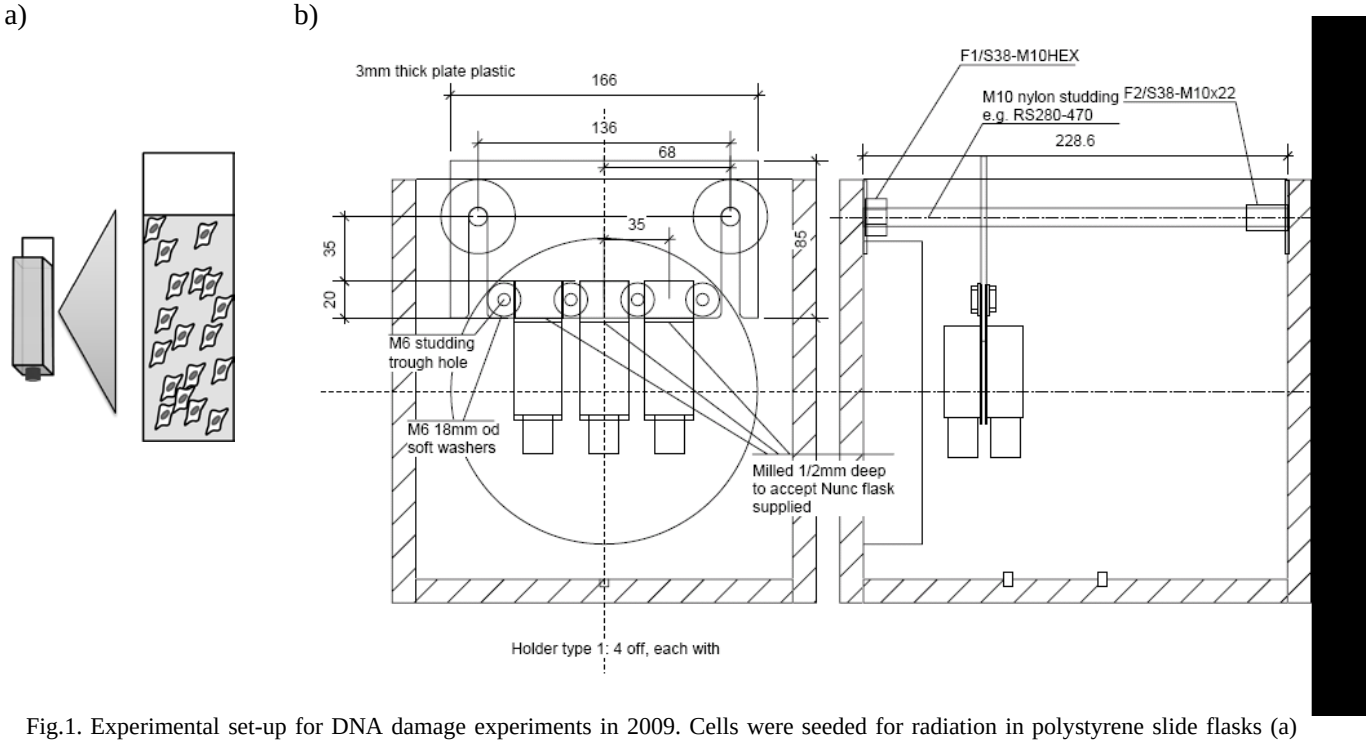

Fig.1. Experimental set-up for DNA damage experiments in 2009. Cells were seeded for radiation in polystyrene slide flasks (a) which were aligned and fixed in position (b) for irradiation with antiprotons. Schematic shows one sample holder as an example only. In the SOBP two flasks were fixed back-to-back as shown, cell monolayers separated by 3mm within the SOBP.

Post radiation treatment

Each set of samples were warmed to 37ºC simultaneously for 1 h in a 95% air/5% CO_2 atmosphere. A time course of development of γ-H2AX foci following cold irradiation of this cell line had previously been established with X-rays in Belfast. All cells were incubated for 1 h post irradiation to allow accumulation of DNA damage sensing proteins. All samples were fixed in ice-cold methanol/acetone (1:1) for 10 min. The fixed cells were washed once in PBS and stored in fresh sterile PBS for transportation to Belfast.

γ-H2AX assay 1) Directly or secondary particle irradiated samples were fixed after 1h incubation. 2) Bystander samples were incubated for 1h with filtered culture media removed from directly irradiated samples. These samples were then also fixed.

Cells were permeablized with 0.5% Triton®X-100 (Sigma-Aldrich) solution in PBS for 20 min at 4ºC; non-specific binding was blocked with 0.2% skimmed milk, 5% foetal bovine serum and 0.1% Triton®X-100 in PBS for 1 h at 4ºC. Cells were incubated for 1 h at 20ºC with anti-phospho-H2AX (mouse monoclonal

antibody, clone JBW301, Upstate Biotechnology). Cells were washed in 0.1% Triton®X-100 solution and then incubated for 1 h at 4ºC with Alexa Fluor® 488 goat anti-mouse cross absorbed antibody (Molecular Probes). Total nuclear DNA was stained with Hoechst stain. Slides were treated with Vectashield mounting media (Vector Labs) and covered with glass cover slips. Images were captured using a Zeiss camera. For directly irradiated samples, cell nuclei were scored only in the centre of the cover slip to ensure all cells within a scored sample had received uniform dose. Images of the cells show the nuclei stained blue and DNA damage (foci) shows up as bright green spots within the nuclei.

Micronucleus assay 1) Directly or secondary particle irradiated samples were treated with cytochalasin-B (0.5µg/ml, Sigma) after 1 h incubation. These were incubated for a further 36 h (time at which maximum number of binucleated cells is seen in this cell line for this assay) prior to fixing. 2) Bystander cells were incubated for 1h with filtered culture media removed from directly irradiated samples prior to addition of cytochalasin B. The fixed cells were washed once in PBS and stored in fresh sterile PBS for transportation to Belfast.
Cells were stained with Acridine orange (Sigma, 25 µl/ml) for 20 min. Washed with fresh PBS x5. Total nuclear DNA was stained with Hoechst stain. Samples were mounted and imaged as for γ-H2AX assay. The numbers of binucleated cells and binucleated cells which had micronuclei were scored within the beam diameter (as determined with gaf chromic film) and outside of the beam.

Plasmid DNA
The plasmid, pcDNA3.1 (Invitrogen, Paisley, UK) was prepared by transformation of a 1 µl aliquot into competent *Escherichia coli* DH5α. A single colony, resulting from this transformation, was picked and grown by shaking overnight at 37°C in 10 ml of LB media supplemented with ampicillin (250 µg/ml). Plasmid was prepared from these cells using a Qiagen Maxi kit according to the manufacturer's instructions. To remove buffer salts (e.g. Tris.HCl) which have previously been shown to scavenge radicals and thus reduce the amount of damage observed. DNA was desalted by using a spin column (Millipore).

Two samples (each approximately 30 µl at a concentration of 450 ng.μl^{-1}) of desalted plasmid solution were exposed to antiprotons (or mock irradiated). The estimated dose received by these samples was 5 Gy and 0 Gy respectively.
A 1 µl aliquot of each irradiated sample was mixed with 5 µl of deionised water and 1 µl of gel loading buffer (0.25% (w/v) bromophenol blue, 40% (w/v) sucrose) and resolved by electrophoresis on a 1%(w/v) agarose:TAE (40 mM Tris-acetate, 1 mM EDTA, pH 8.3) gel containing 0.002%(w/v) ethidium bromide. For comparison, a sample containing 450ng of unirradiated plasmid was electrophoresed alongside the experimental sample. Electrophoresis was carried out in TAE buffer at 100 V (constant voltage) for 40 min and gels imaged using a ChemiDoc XRS gel imager (Biorad, Hercules, CA, USA).
Statistical analysis
Non parametric tests were carried out on data sets with non-Gaussian distributions. Cold and warm control sets (fig.3) were analyzed with the Mann-Whitney U test. Data medians of treated sample sets were initially compared with Kruskal-Wallis non-parametric test, individual median values were compared using Dunn's multiple comparison test.

Results

1. **2008 beam time**

Human fibroblast cells were irradiated with antiprotons at 37°C positioned in plateau and SOBP of the Bragg curve for each dose given. Post irradiation cells were fixed, stained and nuclear DNA damage was scored. Control samples expressed unusually high levels of stress, ~13 foci per nucleus. (fig.2). The mean number of DNA DSBs was observed to increase approximately linearly with dose in the SOBP while the mean number of DSBs observed in the plateau was ~50% of the damage induced in the corresponding SOBP sample. Quantification of secondary particle effects and of bystander effects were not possible as these are expected to be very small effects and require higher sample number and more stringent controls

for increases in DNA damage to be detected. Foci scoring of these samples was carried out and revealed an elevation in damage above that of the control although the error bars were very large as scoring was impeded in many samples due to contamination as a result of a lack of sterile conditions for these biological experiments.

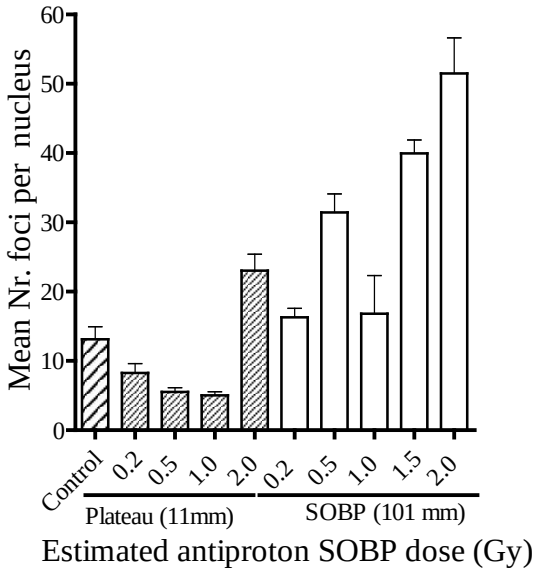

Fig.2. DNA damage increases with antiproton dose in SOBP. Mean number of foci, counted per cell over 50 cells per sample, increased approximately linearly with dose. Error bars indicated SEM of one sample.

2. 2009 beam time

Comparison of this years controls with last years

Control samples displayed very low levels of DNA damage. Mean number foci from scoring of two independent samples of 200 cells was 1.7 as also measured under standard cell culture conditions in our laboratory in Belfast. Mean number foci per nucleus in the 2008 control was 13 (fig.3). Availability of sterile cell culture facilities, as well as the new experimental design, this year has also ensured that not a single sample was contaminated despite being completely submerged in the water phantom for irradiations.

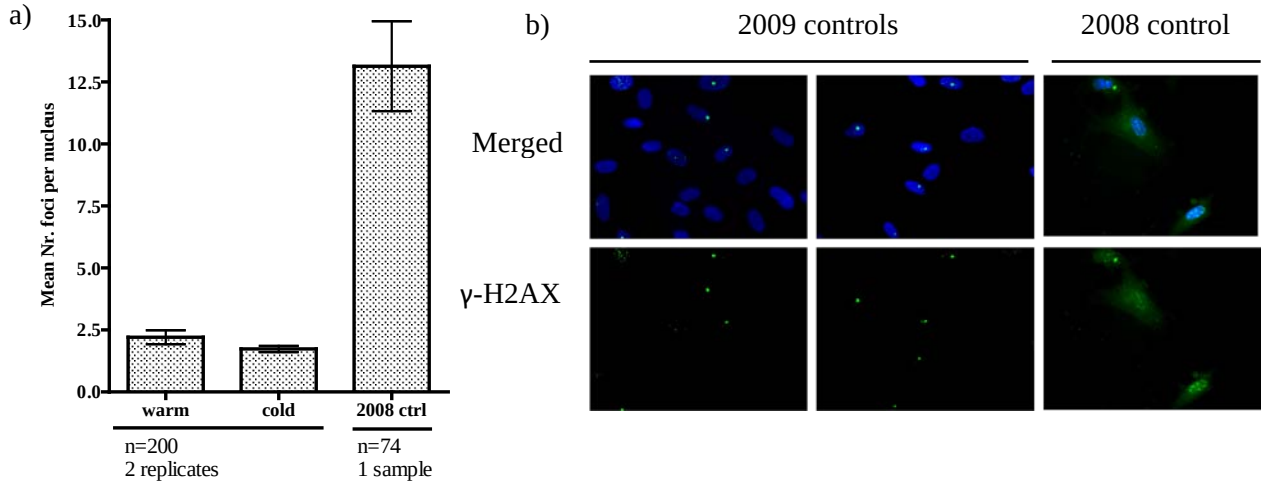

Fig.3. Non-irradiated control samples. A) Foci score indicates level of endogenous DNA damage significantly decreased in control samples this year relative to last years samples and error bars decreased. Medians for warm and cold controls were not significantly different. Error bars indicate SEM. B) Low levels of endogenous γ-H2AX foci in controls shown by immunofluorescence.

Analysis of immediate DNA damage response to antiproton irradiation: γ-H2AX assay

a) Response to direct irradiation

Foci were scored in cells across the diameter of a 6mm spot on the sample slides which was positioned according to the gaf chromic film on each sample. All plateau samples contained many cells with bright and well defined foci. The mean number of foci in plateau samples was observed to be dose responsive. SOBP samples contained many cells which displayed very dense or clustered DNA double strand breaks (observed at x63 magnification) (fig.4b). Plateau samples did not show similar clustered foci regardless of dose or total number of foci (fig.4b). This indicates complex DNA damage caused by the antiproton annihilation. Number of foci per cell is also dose dependent in the SOBP. The experimental set up allowed two samples to be placed back to back (cell monolayers ~ 3mm apart) in the SOBP. The scoring of foci revealed that only in the '0.5Gy' samples was the difference in damage significant. This may be attributed to relatively uneven SOBP predicted for this low dose point. All other doses were given with a flat SOBP.

In addition to scoring the effects of direct irradiation, distance response perpendicular to the beam has also been recorded at 3mm increments away from the edge of the beam (assuming diameter of 6mm). At 3mm mean foci number drops dramatically and by 18mm the level of damage is similar to that in the controls (fig.4b). This trend will be analysed against the dose response measured by the gafchromic films.

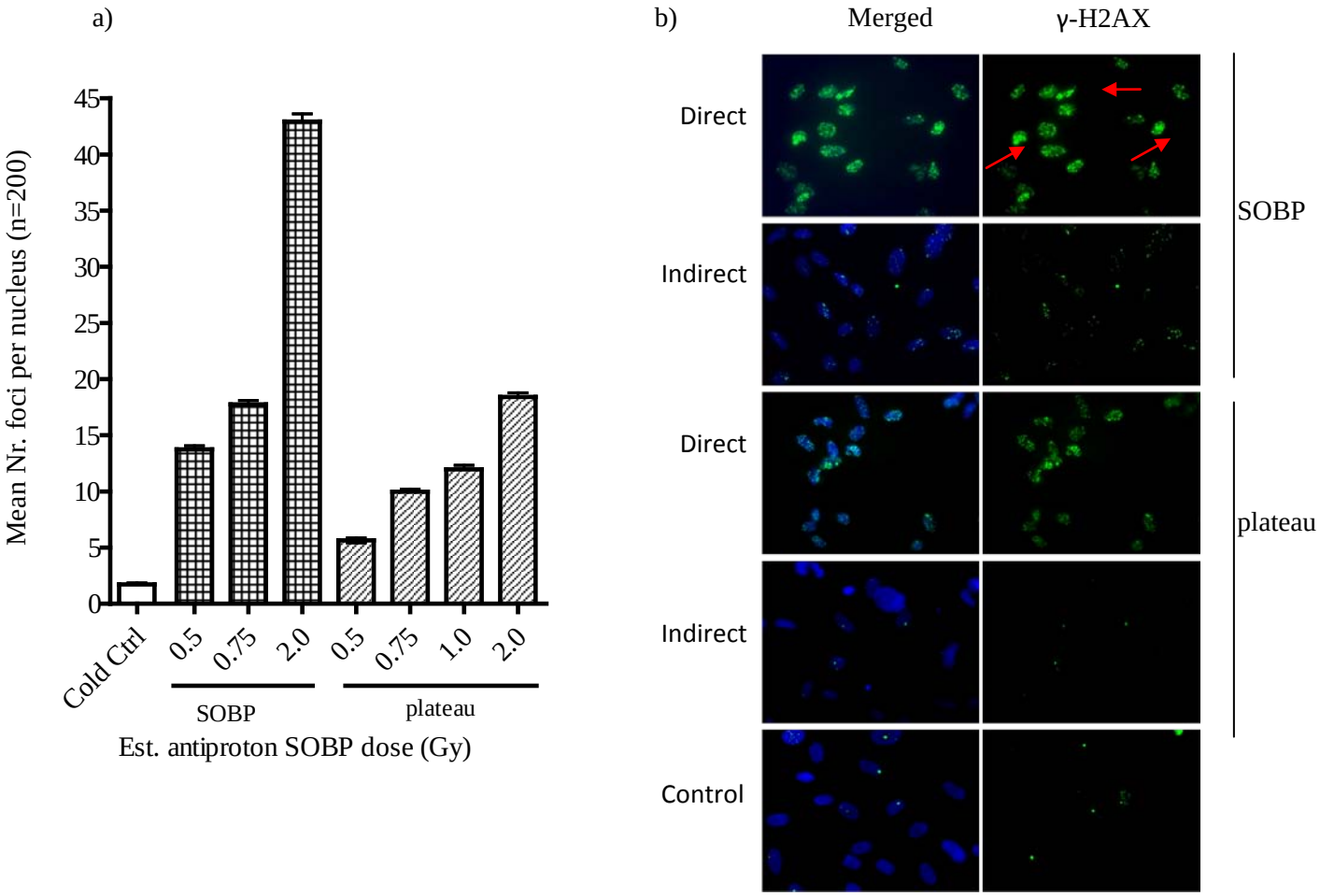

Fig.4. DNA damage dose response to antiproton SOBP and plateau. A) Mean number of foci per nucleus (200 nuclei per sample) increases with dose. B) Immunofluorescence images representative of foci distribution in 2Gy samples in SOBP and plateau. 'Direct' indicates cells which were placed in the beam path while 'Indirect' indicates cells within the same sample which were

out of the beam path (not traversed by antiprotons). The mean foci number in these regions was similar to that of the control samples. Non-irradiated controls were otherwise treated same as irradiated samples. Red arrows indicate nuclei with clustered foci.

Indirect effects of antiproton irradiation

Scoring of γ-H2AX foci in bystander samples revealed a modest increase in DNA damage relative to the control samples. This effect does not, however, appear to be dose dependent (fig.5a). These cells were incubated with culture media from samples that were irradiated with antiprotons in the SOBP. It could be that concentration of cytokines in the transferred media was too low to produce a strong response in bystander cells which were a much larger population than that which was directly irradiated. Further comparison with X-ray radiation is required to corroborate this analysis.

Analysis of secondary particle samples (see fig.5b) which were placed in the phantom at the time of irradiation and fixed adjacent to the directly irradiated samples display no significant increase in damage relative to the controls at this time. A strong response was not expected at the distances measured due to the relatively low dose of secondary particles which drops off quickly with distance from the annihilation vertex. Only cells adjacent to the 2Gy sample gave a response that was significantly different to the controls. The data seem to indicate a dose dependent response; this will be confirmed with data from 5Gy samples which has not yet been scored.

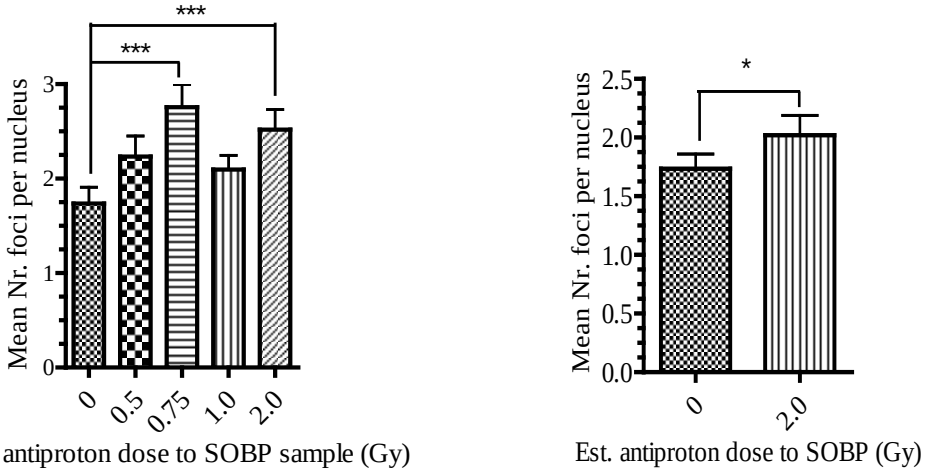

Fig.5. Indirect effects of antiproton radiation. A) Bystander experiment, results from two independent samples, error bars indicate standard deviation from the average of the two means; B) secondary particle experiment, results from one experiment, error bars indicate SEM of 200 cells per sample.'***' indictes P value of less than 0.001, '*' indicates P value less than 0.05.

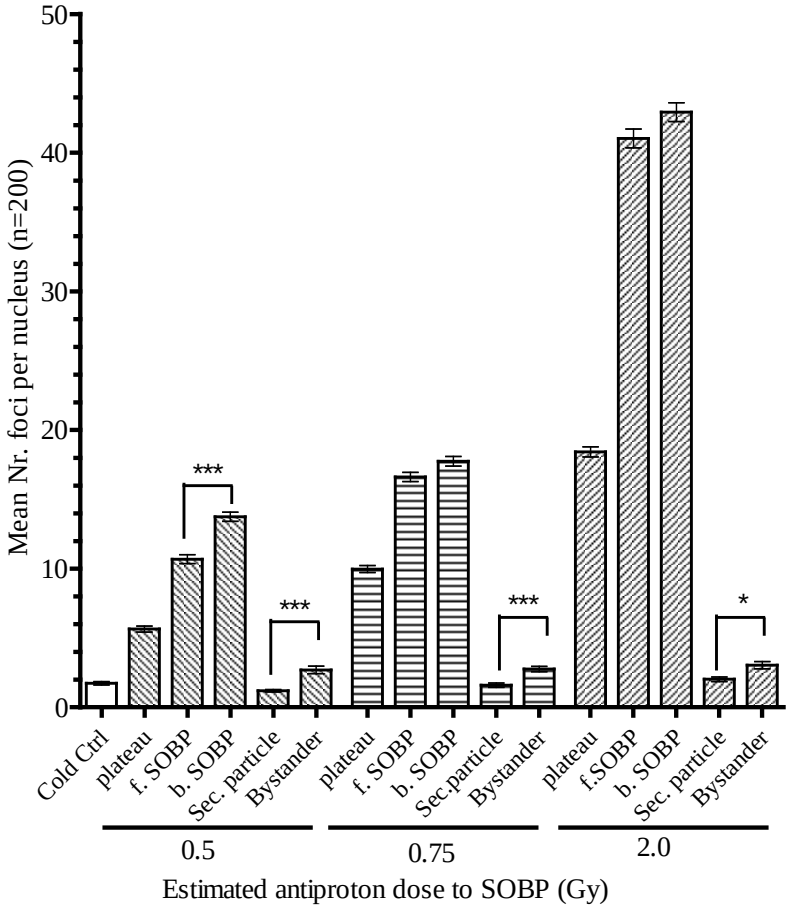

Fig.6. For each dose there are five sample sets for the γ-H2AX assay each of which provides different information about the effects of either direct or indirect antiproton irradiation. Two sample were placed in the Bragg peak for each dose-labeled here as 'f.SOBP' and 'b.SOBP' (f: front, b: back) where f was the sample closer to the plateau. Mean foci number for f.SOBP and b.SOBP was only significantly different in the 0.5Gy dose samples, $P<0.001$). Results are for one experiment, error bars are SEM for 200 cells per sample.

Analysis of longer term damage: Micronucleus assay

In non-irradiated control samples binucleated cells (BN) were counted within a sample spot of 6mm diameter. The percentage of BN in the control population was ~40%. Using this assay micronucleated cells are usually scored from 1000 BN. This was not possible here due to the small sampling radius.

In samples which received antiproton SOBP irradiation there is little if any evidence of cells attempting division. Samples which received antiproton SOBP irradiation had 8% and 5% BN for 1 and 2 Gy respectively (fig.7a). Of the BN present in each irradiated sample 39% and 68% had micronuclei, compared to 1.4% in control sample (fig.7b).

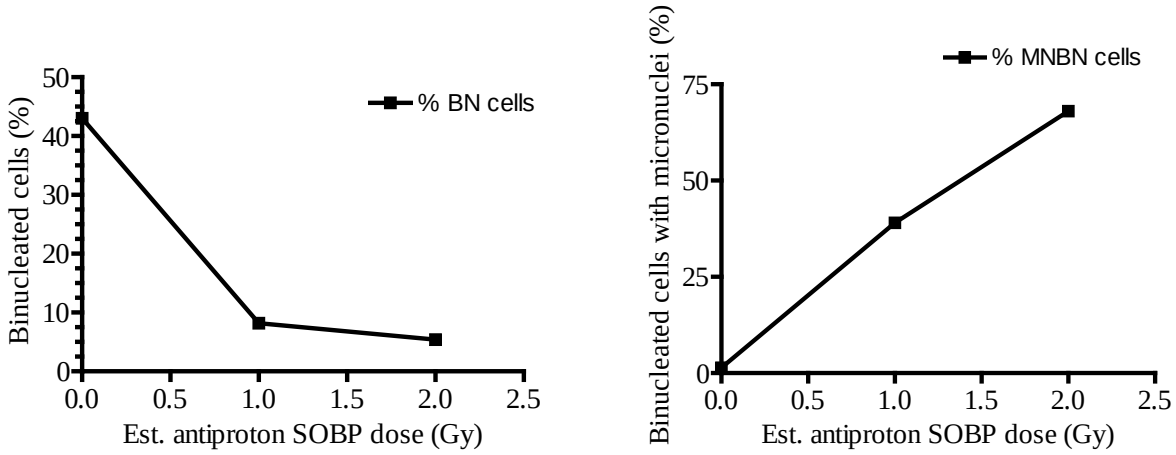

Fig.7. Micronuclei assay. A) Percentage of sample population with binucleated cells decreases with SOBP antiproton radiation. B) Percentage of binucleated cells containing micronuclei increases with antiproton dose.

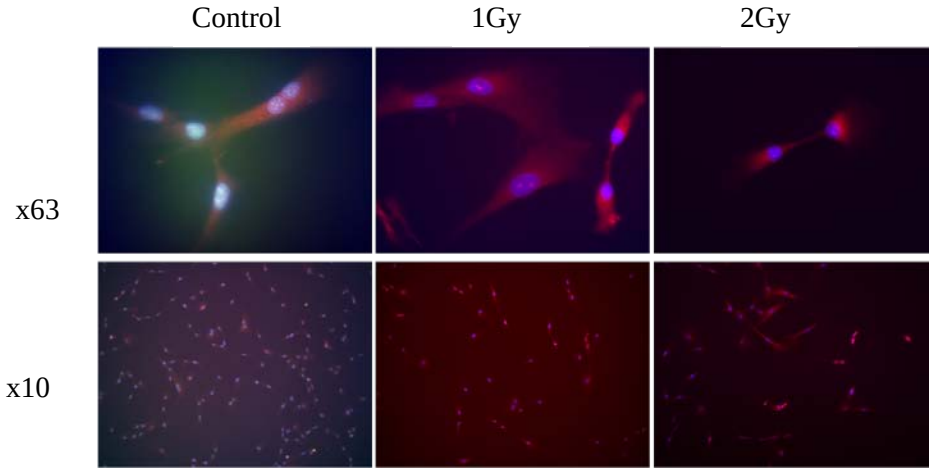

Fig.8. Immunofluorescence images of cells treated with cytochalasin B for 36h after antiproton treatment.

Previous experiments using this assay for the AGO1522B cell line have demonstrated similar or lower binucleation in non-irradiated control samples. A repeat of these experiments with X-rays is planned following the same protocols as for antiproton experiments. Initial data suggests that the impact on cell survival is strongly linked to radiation quality.

The level of binucleation provides only information on the potential for cell survival. Of more importance for these experiments are those cells which survived antiproton irradiation and display evidence of genetic instability. Figure 7b suggests that loss of genetic integrity is dose dependent for SOBP irradiation. Analysis of a 5Gy SOBP-irradiated sample is anticipated to show a complete loss of binucleation.
More interesting will be the MN induction in the plateau as there little cell killing is expected. Ultimately it will be the sub-lethal damage in the entrance channel which limits the outcome of any radiation treatment.

Gaf chromic film

Water resistant strips of gaf chromic film were attached to the back of directly irradiated sample flasks. The immediate purpose was orientation of the region of the samples that was directly in the beam path. The films can also provide some information on beam shape and dose deposition for the dose range in both SOBP and plateau.

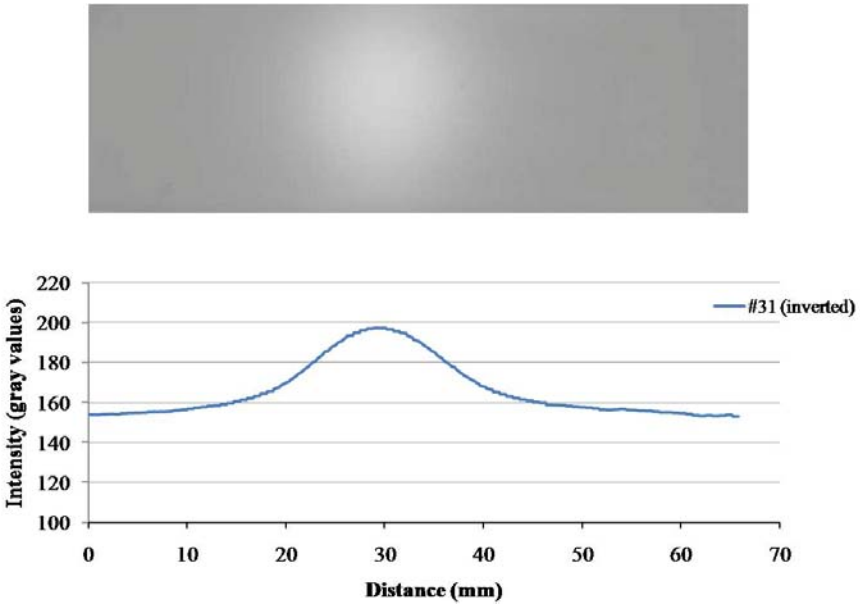

Fig.9. A scan of the gaf chromic film which had been attached to sample 31 at the time of antiproton irradiation was inverted and subsequent intensity profile plotted using Image J software package.

Antiproton induced damage in plasmid DNA

Desalted plasmid DNA received estimated antiproton SOBP dose of 5Gy. Non-irradiated control sample was run on gel alongside the treated sample. Alongside the markers (run in lane 1), control sample (lane2) contains mostly super coiled DNA and a small amount of open circle DNA. Irradiated sample (lane3) has lost all super coiled DNA (to the level detectable with this assay) and instead contains open circular and linear DNA. This pilot experiment indicates that our plasmid DNA preparation has sufficient sensitivity to be used in basic studies of antiproton-induced damage to biomolecules.

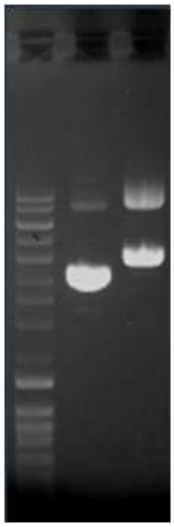

Fig.9. Antiprotons cause plasmid DNA damage. A) Plasmid gel with ladder (lane 1) untreated plasmid is mostly of the super coiled form with small amount of open circular (lane 2) antiproton treated plasmid DNA is in the form linear (double strand breaks) and open circle (single strand breaks) with no super coiled DNA detectable (lane 3).

Summary

- Collaboration with O. Hartley at Geneva Medical University for use of biological facilities before and during the beam time contributed greatly to the successful completion of a large sample set for several different experiments. This has demonstrated the possibility for more complex biological experiments in the future aided by that collaboration.
- Ratio of DNA damage in the peak compared to the plateau gives an indication of an antiproton RBE for DNA damage induction which could be compared to RBE obtained from cell survival data (although cell lines differ).
- Data collection from both micronucleus and γ-H2AX assays are still on going and has already provided an indication of short and long term effects on cellular DNA.
- Indirect effects measured are very small and these will require specific statistical analyses to determine their significance.
- Irradiation of desalted plasmid DNA has demonstrated a response to clinically relevant doses which was not achieved during the beam time of 2007. As plasmid DNA gels can be quantified this success suggests a possible future dosimeter for particle radiation which may be developed in future beam times.

Future Experiments

1. **Genetic instability**

Up to now evidence from investigations into antiproton induced cell damage has indicated that exposed cells experience either lethal or non lethal damage, where lethality is linked strongly to radiation LET.
We are interested to know with what frequency there is genetic instability in cells which survive an antiproton dose.
It has been shown that antiproton traversal in the plateau dose result in elevated DNA damage and that impact for Bystander signaling and secondary particles near the SOBP induces a level of damage above that of the control. Clonogenic survival data (at least in V79cells) would indicate that damage expressed in the plateau region is non-lethal. The next question then is how successfully the non-lethal damage is repaired and at what rate is genetic instability created in the original cells and to what extent is this transmitted in their progeny.

2. **Effectiveness of antiproton SOBP in hypoxic cells**

It has been proposed that the high LET antiproton Bragg peak would potentially increase cell killing ability in hypoxic tissues. We would like to test this hypothesis in a cell model under hypoxia.

References

1. Bryant, P.E. International Journal of Radiation Biology 48 (1985): 55-60
2. Rogakou, E. P., D. R. Pilch, A. H. Orr, V. S Ivanonva, and W. M. Bonner. The Journal of Biological Chemistry 273, no. March (1998): 5858-5868.
3. Castedo, M.,Perfettini,J., Roumier, T., Andreau, K., Medema, R., Kroemer, G. Oncogene, 23 (2004) 2825-2837.
4. Molz, L., Boohe, L.H., Young, P., Beach, D. Genetics, (1989) 773-782.
5. Mothersill, C., and Seymour, C.B. Radiation Research 149 (1998): 256-262.
6. Seymour, C. B., Carmel. Mothersill, C. Radiation Research 153 (2000): 508-511.
7. Mancuso, M, and et al. PNAS, USA 105 (2008): 12445-12450.
8. Wyer JA, Butterworth KT, Hirst DG, Latimer CJ, Montenegro EC, Shah MB, Currell FJ (2009) Phys Med Biol. 54:4705-4721.
9. Folkard M, Prise KM, Brocklehurst B, Michael BD (1999) *J. Phys. B: At. Mol. Opt. Phys.* 32:2753-2761.